

Noisy Monitored Quantum Circuits

Shuo Liu,^{1,2} Shao-Kai Jian,^{3,*} and Shi-Xin Zhang^{4,†}

¹*Department of Physics, Princeton University, Princeton, NJ 08544, USA*

²*Institute for Advanced Study, Tsinghua University, Beijing 100084, China*

³*Department of Physics and Engineering Physics,
Tulane University, New Orleans, Louisiana 70118, USA*

⁴*Institute of Physics, Chinese Academy of Sciences, Beijing 100190, China*

(Dated: December 23, 2025)

Noisy monitored quantum circuits have emerged as a versatile and unifying framework connecting quantum many-body physics, quantum information, and quantum computation. In this review, we provide a comprehensive overview of recent advances in understanding the dynamics of such circuits, with an emphasis on their entanglement structure, information-protection capabilities, and noise-induced phase transitions. A central theme is the mapping to classical statistical models, which reveals how quantum noise reshapes dominant spin configurations. This framework elucidates universal scaling behaviors, including the characteristic $q^{-1/3}$ entanglement scaling with noise probability q and distinct timescales for information protection. We further highlight a broad range of constructions and applications inspired by noisy monitored circuits, spanning variational quantum algorithms, classical simulation methods, mixed-state phases of matter, and emerging approaches to quantum error mitigation and quantum error correction. These developments collectively establish noisy monitored circuits as a powerful platform for probing and controlling quantum dynamics in realistic, decohering environments.

I. INTRODUCTION

Random quantum circuits (RQCs) [1], composed of randomly chosen unitary gates, have emerged as a universal tool bridging quantum many-body physics, quantum information, and quantum computing. In the context of quantum many-body physics, RQCs provide a theoretically tractable minimal model for exploring generic aspects of quantum chaos, quantum thermalization, information scrambling, symmetry restoration, and so on [2–21]. RQCs have also been widely applied in quantum sciences, including approximate unitary designs [22–30], benchmarking for quantum supremacy [31–35], shadow tomography [36, 37] and variational quantum algorithms [38, 39].

An important extension of RQCs is the monitored quantum circuits, where unitary dynamics are interspersed with quantum measurements [40–42]. In these monitored quantum circuits, the competition between unitary entanglement generation and measurement-induced disentanglement leads to a dynamical phase transition: the steady state entanglement obeys volume law when the measurement probability p_m is below the critical probability p_m^c while it obeys area law when $p_m > p_m^c$ [40–42]. This dynamical phase transition is known as measurement-induced phase transitions (MIPTs) [40–42] and has been extensively investigated in monitored quantum circuits [43–72]. MIPTs as well as the associated measurement-induced criticality have also been substantially explored in general monitored quantum many-body systems, e.g., monitored SYK

model, monitored free fermion and monitored critical ground states [73–112]. Thanks to the rapid development of quantum simulation hardware, MIPTs have also been demonstrated in several experiments on quantum devices [113–117].

However, real quantum systems inevitably suffer from environmental decoherence, which fundamentally alters the nature of quantum dynamics from pure-state evolution to mixed-state density matrix evolution. This fact motivates the study of noisy (monitored) quantum circuits. Due to intrinsic randomness, noisy quantum circuits can be mapped to classical statistical models in one higher dimension [118–125]. In this statistical picture, while unitary dynamics promotes permutation symmetry among replicas, the quantum noise plays the role of symmetry breaking field that explicitly favor the identity permutation, thereby competing with entanglement generation. Building on this mapping, the entanglement structure and its universal scaling laws [119–128], the error correction capacity [124, 129–132], and the classical simulation hardness or nonstabilizerness [133–140] of noisy (monitored) quantum circuits have been extensively explored through both theoretical analysis and numerical simulation.

Beyond the minimal models of brick-wall random circuits, many variations have been explored, motivated by both theoretical considerations and experimental constraints. For instance, imposing conservation laws leads to new dynamical phase transitions, including the charge-sharpening phase transition in symmetric quantum circuits [141–145] with distinct entanglement entropy growth dynamics [146, 147]. Furthermore, introducing measurement feedback allows for the absorbing phase transition, a distinct critical phenomenon that can be detected by linear observables [145, 148–151]. Other

* sjian@tulane.edu

† shixinzhang@iphy.ac.cn

model variations investigate the effects of spatiotemporal structure and alternative monitoring protocols, including circuits incorporating temporally correlated randomness [125, 152–154], long-range interactions [147, 155–158], measurement-only systems [159–170], weak measurements [171–173], and other geometric structures such as quantum trees [174, 175].

In addition to being a useful tool for studying quantum dynamics, noisy quantum circuits have also inspired developments across a wide range of fields, including variational quantum algorithms [176–179], classical simulation [35, 180–192], mixed-state phases of matter [193–207], and quantum error mitigation and correction [208–215]. Therefore, these models also provide a valuable framework that connects different fields and inspired practical applications.

This review provides a unified overview of recent progress in noisy monitored quantum circuits. We begin with basic concepts, including the circuit setup, the relevant observables, and the mapping to classical statistical models. We then discuss the entanglement structure of steady states of the noisy monitored quantum circuits, followed by a discussion on the information protection capabilities of such circuits. Next, we present the noise-induced phase transitions that arise in these systems, including noise-induced entanglement phase transition, coding transition, and complexity transition. Finally, we survey a range of applications of noisy monitored quantum circuits across quantum information science and quantum many-body physics.

II. SETUP OF NOISY MONITORED QUANTUM CIRCUITS

We begin by outlining the basic setup of the noisy monitored quantum circuits and the observables used for the investigation of entanglement and information dynamics.

A. Circuit setup

For concreteness, we consider the one-dimensional noisy monitored quantum circuits where the unitary gates are arranged in a brick-wall structure. This 1D system consists of L qudits, each with local Hilbert-space dimension d where $d = 2$ corresponds to qubits.

To probe entanglement generation, the system is typically initialized in a product state,

$$|\psi(0)\rangle = |0\rangle^{\otimes L}, \quad (1)$$

which contains no initial entanglement. Time evolution proceeds in discrete layers, as illustrated in Fig. 1 (a). Each layer consists of a brick-wall arrangement of random two-qudit unitary gates acting with periodic boundary conditions. Following the unitary layer, both projective measurements and quantum noise channels act independently on every qudit with probabilities p_m and q ,

respectively. Note that the critical measurement probability reported in Ref. [58] is $p_m^c = 0.15995$, which is half of the value in the present setup. This difference arises because their circuit applies a single measurement layer for each (even or odd) unitary layer. We denote the total number of time steps by T . Note that in this case there is no correlation between quantum noise events at different space-time locations, and the occurrence probability of quantum noise is independent of system size. We will also discuss the effects of temporal correlations between noise events shown in Fig. 1 (b) (see Sec. V), as well as scenarios in which the occurrence probability becomes system-size dependent (see Sec. VI).

Noisy monitored circuits contain four distinct sources of randomness:

- (1) independently Haar-random two-qudit unitary gates,
- (2) random space–time locations of quantum noises,
- (3) random space–time locations of projective measurements,
- (4) intrinsically random measurement outcomes dictated by the Born rule.

A single realization of all these random elements defines a *trajectory*. For any observable of interest, we first compute its value for each trajectory and subsequently average over many such trajectories. For nonlinear quantities such as von Neumann entropy, the order of averaging is essential, and we follow the convention described above.

In practice, we choose the evolution time T long enough for entanglement-related observables to saturate, indicating that the system has reached a steady state. For monitored circuits without additional quantum noise, this typically requires $T \sim L$ [40–42], although noise can modify this scaling.

B. Entanglement-related observables

Having introduced the circuit setup, we now describe the observables used to characterize entanglement in noisy monitored quantum circuits. Because quantum noise inevitably reduces the purity of the state, the time-evolved density matrix is generically mixed. In such settings, conventional entanglement measures based on subsystem von Neumann entropy are no longer reliable to distinguish quantum correlations from classical mixing [216, 217]. Accordingly, we employ entanglement measures and information-theoretic quantities that remain meaningful for mixed states.

Logarithmic entanglement negativity. To quantify bipartite entanglement between the left (A) and right (B) halves of the system, we use the logarithmic entanglement negativity [160, 218–226], defined as

$$E_N = \log \|\rho^{T_B}\|_1, \quad (2)$$

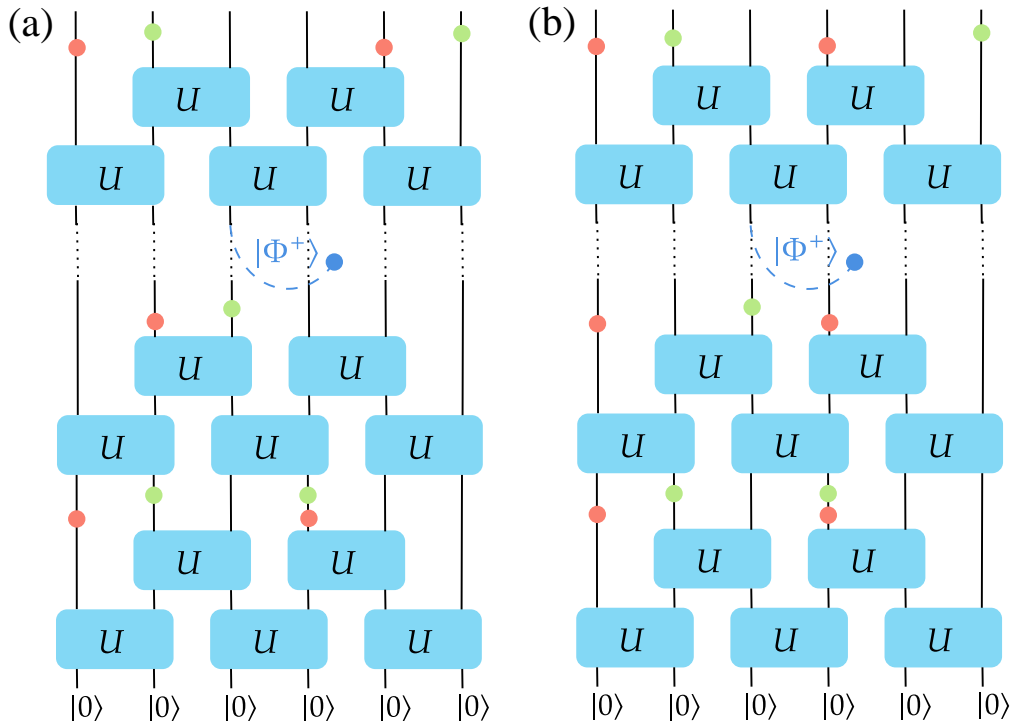


FIG. 1: *Setup of noisy monitored quantum circuits.* (a) Temporally uncorrelated and (b) correlated quantum noises (red circles). Projective measurements are indicated by green circles. In the steady state encoding scheme, after the system reaches its steady state, a reference qudit (blue circle) is introduced and maximally entangled with the central qudit to form a Bell pair, thereby encoding one-qudit quantum information into the circuit. Reprinted with permission from Ref. [125], Copyright (2024) by the American Physical Society.

where ρ^{TB} is the partial transpose of the density matrix with respect to subsystem B , and $\|\cdot\|_1$ is the trace norm. Logarithmic entanglement negativity is widely used in the study of monitored circuits [119, 160] and provides a robust diagnostic of entanglement scaling in the presence of both noise and measurements.

Mutual information. A complementary diagnostic is the mutual information between A and B ,

$$I_{A:B} = S_A + S_B - S_{AB}, \quad (3)$$

where $S_\beta = -\text{tr}(\rho_\beta \ln \rho_\beta)$ denotes the von Neumann entropy of subsystem β with reduced density matrix ρ_β . Although mutual information receives contributions from both quantum and classical correlations, it exhibits scaling behavior similar to that of logarithmic entanglement negativity in the investigation of noisy quantum circuits and is particularly natural in the statistical-model description developed later.

C. Information-related observables and encoding schemes

Beyond characterizing entanglement dynamics, it is also essential to quantify the ability of noisy monitored

quantum circuits to preserve quantum information. In the presence of quantum noise, any encoded information is gradually degraded and eventually leaks into the environment. However, how the information-protection timescale depends on the properties of the noise, including its type, occurrence probability, and temporal correlations, is far from obvious and requires a careful operational definition.

To address this question, we consider a standard information-encoding protocol. At a designated time T_e , we introduce a reference qudit R , initially prepared in the state $|0\rangle$. This reference qudit is then maximally entangled with a chosen system qudit through the creation of a Bell pair. Because the circuit is implemented with periodic boundary conditions, the specific spatial location of the system qudit is not important; in all cases, this procedure encodes one qudit of quantum information into the evolving circuit.

We examine two natural encoding schemes:

- (1) *Steady-state encoding shown in Fig. 1*, where the Bell pair is inserted at a time $T_e > T$, after the circuit has already relaxed to its steady state (see Sec. V).
- (2) *Initial-state encoding shown in Fig. 10*, where the Bell pair is inserted at $T_e = 0$ before the circuit

evolution begins (see Sec. [VIB](#)).

Following the encoding, the system continues to evolve under the noisy monitored dynamics. The central quantity of interest is the characteristic timescale over which the initially encoded information becomes irretrievable due to decoherence.

To quantify how much information remains within the system at time t , we evaluate the mutual information between the entire system AB and the reference qudit R :

$$I_{AB:R} = S_{AB} + S_R - S_{ABUR}, \quad (4)$$

where S also denotes the von Neumann entropy. Immediately after encoding, the formed Bell pair ensures that

$$I_{AB:R} = 2 \log_d d = 2, \quad (5)$$

reflecting the full retention of one qudit of quantum information. Note that the logarithm is taken with base d throughout this work. In the long-time limit, the decay of this quantity to zero,

$$I_{AB:R} \rightarrow 0, \quad (6)$$

signifies that the encoded information has been completely lost to the environment. Tracking the decay of $I_{AB:R}$ therefore provides a direct operational measure of the information-protection capability of noisy monitored quantum circuits.

III. MAPPING TO STATISTICAL MODELS

In this section, we introduce the mapping between noisy monitored quantum circuits and effective classical statistical models in one higher dimension [[119–125](#)]. This mapping provides a unifying framework for understanding entanglement quantities which are encoded in the free energy of the corresponding statistical model. For clarity, we first review the mapping for noiseless random unitary circuits and then describe how quantum noise and measurements modify the effective classical model. Throughout this subsection, we focus primarily on the von Neumann entropy and mutual information $I_{A:B}$ and $I_{AB:R}$, while the logarithmic entanglement negativity can be treated similarly [[120, 125](#)].

A. Mapping for noiseless random circuits

Consider a brick-wall circuit composed of Haar-random two-qudit gates, as illustrated in Fig. [2](#) (a). After T discrete time steps, the system evolves into

$$\rho^{(T)} = \left(\prod_{t=1}^T \tilde{U}_t \right) \rho_0 \left(\prod_{t=1}^T \tilde{U}_t \right)^\dagger, \quad (7)$$

where $\rho_0 = |\psi(0)\rangle\langle\psi(0)|$ is the density matrix of initial state, \tilde{U}_t denotes the unitary layer at time step t and is given by

$$\tilde{U}_t = \prod_{i=0}^{\frac{L-2}{2}} U_{t,(2i+2,2i+3)} \prod_{i=0}^{\frac{L-2}{2}} U_{t,(2i+1,2i+2)}. \quad (8)$$

We set L to be even without loss of generality, and assume the periodic boundary condition, $U_{t,(L,L+1)} = U_{t,(L,1)}$. To perform the Haar average, we vectorize ρ and introduce r replicas (the meaning naturally emerges later):

$$|\rho^{(T)}\rangle^{\otimes r} = \prod_{t=1}^T [\tilde{U}_t \otimes \tilde{U}_t^*]^{\otimes r} |\rho_0\rangle^{\otimes r}. \quad (9)$$

Each random two-qudit unitary gate $U_{t,(i,j)}$ can be averaged independently [[3, 4, 9, 46, 47, 119, 141, 227, 228](#)], giving rise to

$$\mathbb{E}_{\mathcal{U}}(U \otimes U^*)^{\otimes r} = \sum_{\sigma, \tau \in S_r} \text{Wg}_{d^2}^{(r)}(\sigma\tau^{-1}) |\tau\rangle\langle\sigma|, \quad (10)$$

where Wg is the Weingarten function, σ, τ are permutation spins in the permutation group S_r of dimension r . In the large- d limit, the Weingarten function has an asymptotic expansion [[9, 228](#)]

$$\text{Wg}_{d^2}^{(r)}(\sigma) = \frac{1}{d^{2r}} \left[\frac{\text{Moeb}(\sigma)}{d^{2|\sigma|}} + O(d^{-2|\sigma|-4}) \right], \quad (11)$$

where $|\sigma|$ is the number of transpositions required to construct σ from the identity permutation spin \mathbb{I} , and $\text{Moeb}(\sigma)$ refers to the Möbius number of a permutation σ .

After performing the Haar average, the permutation spins become the effective degrees of freedom, enabling the dynamics of the random quantum circuit to be mapped onto a classical statistical model in one higher dimension. The partition function Z of this model is obtained by summing over all permutation-spin configurations, where the weight of each configuration factorizes into contributions from diagonal and vertical bonds, as illustrated in Fig. [2](#).

The diagonal bond weight corresponds to the overlap between two diagonally adjacent permutation spins,

$$w_d(\sigma, \tau) = \langle\sigma|\tau\rangle = d^{r-|\sigma^{-1}\tau|}, \quad (12)$$

while the vertical bond weight is determined by the Weingarten function introduced in Eq. [\(11\)](#). Because the Möbius function $\text{Moeb}(\sigma)$ appearing in the Weingarten expansion can take negative values [[228](#)], the resulting bond weights are not manifestly positive. To obtain a well-defined classical model with positive statistical weights, we integrate out the intermediate τ spins, which yields effective three-body weight $W^0(\sigma_1, \sigma_2; \sigma_3)$ (see Fig. [2](#)) on downward triangles. In the large- d limit, the leading contributions are

$$W^0(\sigma, \sigma; \sigma) \sim d^0, \quad (13)$$

$$W^0(\sigma', \sigma; \sigma) \sim d^{-|\sigma'^{-1}\sigma|}, \quad (14)$$

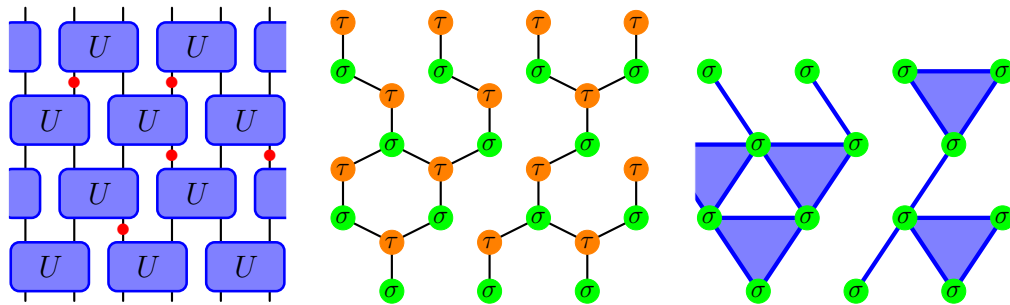


FIG. 2: *Outline of the mapping to the effective statistical model.* Starting from the bulk circuit (left), averaging over the unitary gates in Eq. (10) introduces two permutation spins, σ and τ , for each two-qubit gate (center). Vertical bonds are weighted by the Weingarten function in Eq. (11), while diagonal bonds are weighted according to Eq. (12) in the absence of measurements. When a measurement occurs, the corresponding diagonal bonds are removed. After integrating out the τ spins, we obtain a model with three-body weights on downward-facing triangles (right) in the absence of measurements; these three-body weights reduce to two-body weights when one of the bonds is measured. Reprinted with permission from Ref. [119], Copyright (2022) by the American Physical Society.

indicating that neighboring permutation spins prefer to align, while domain walls cost an energetic penalty proportional to the permutation distance. Thus, the resulting statistical model is effectively ferromagnetic, and its dominant configuration is the minimum-energy arrangement of permutation spins consistent with the imposed boundary conditions.

B. Entanglement entropy from free energy

We now outline how von Neumann entropy is extracted from the free energy of the statistical model. The von Neumann entropy of a subsystem β can be written as

$$S_\beta = \lim_{n \rightarrow 1} S_\beta^{(n)} = \lim_{n \rightarrow 1} \frac{1}{1-n} \mathbb{E}_{\mathcal{U}} \log \frac{\text{tr} \rho_\beta^n}{(\text{tr} \rho)^n}. \quad (15)$$

Here $S_\beta^{(n)}$ is the n -th Rényi entropy. In the replicated Hilbert space, $\text{tr}(\rho_\beta^n)$ corresponds to inserting a cyclic permutation C_β on region β , while $(\text{tr} \rho)^n$ corresponds to identity permutations. Therefore,

$$\begin{aligned} S_\beta^{(n)} &= \frac{1}{1-n} \mathbb{E}_{\mathcal{U}} \log \frac{\text{tr} \rho_\beta^n}{(\text{tr} \rho)^n} \\ &= \frac{1}{1-n} \mathbb{E}_{\mathcal{U}} \log \frac{\text{Tr}((C_\beta \otimes I_{\bar{\beta}}) \rho^{\otimes n})}{\text{Tr}((I_\beta \otimes I_{\bar{\beta}}) \rho^{\otimes n})} \\ &= \frac{1}{1-n} \mathbb{E}_{\mathcal{U}} \log \frac{Z_\beta^{(n)}}{Z_0^{(n)}}, \end{aligned} \quad (16)$$

where $Z_\beta^{(n)}$ and $Z_0^{(n)}$ are partition functions with boundary conditions $C_\beta \otimes I_{\bar{\beta}}$ and $I_\beta \otimes I_{\bar{\beta}}$ respectively.

To move the Haar average inside the logarithm, we

introduce an additional replica index k [229, 230]:

$$\mathbb{E}_{\mathcal{U}} \log Z_\beta^{(n)} = \lim_{k \rightarrow 0} \frac{1}{k} \log Z_\beta^{(n,k)}, \quad (17)$$

$$\mathbb{E}_{\mathcal{U}} \log Z_0^{(n)} = \lim_{k \rightarrow 0} \frac{1}{k} \log Z_0^{(n,k)}. \quad (18)$$

The replicated partition function $Z_\beta^{(n,k)}$ corresponds to a classical spin model with fixed top boundary condition $\mathbb{C}_\beta = C_\beta^{\otimes k}$, while $Z_0^{(n,k)}$ corresponds to a uniform identity boundary. Consequently, the entropy reduces to a free-energy difference:

$$\begin{aligned} S_\beta &= \lim_{n \rightarrow 1} \lim_{k \rightarrow 0} \frac{1}{k(1-n)} \log \frac{Z_\beta^{(n,k)}}{Z_0^{(n,k)}} \\ &= \lim_{n \rightarrow 1} \lim_{k \rightarrow 0} \frac{F_\beta^{(n,k)} - F_0^{(n,k)}}{k(n-1)}. \end{aligned} \quad (19)$$

We note that the free energy $F^{(n,k)}$ is proportional to the length of the domain wall, with a unit energy cost of $k(n-1)$. As a result, the combination $F^{(n,k)}/[k(n-1)]$ becomes independent of the replica indices (n, k) . Consequently, the replica limits required to extract the von Neumann entropy in Eq. (19) can be taken smoothly.

Moreover, because the bottom boundary is free (reflecting the product initial state), the dominant configuration contributing to $F_0^{(n,k)}$ is the uniform identity configuration, giving $F_0^{(n,k)} = 0$. Thus the von Neumann entropy is fully determined by the free energy $F_\beta^{(n,k)}$. More importantly, in the large- d limit, partition function $Z_\beta^{(n,k)}$ as well as the free energy $F_\beta^{(n,k)}$ are determined by the single dominant spin configuration, which greatly simplifies the analytical analysis. This construction establishes the statistical-model framework used to analyze both noiseless and noisy monitored quantum circuits.

To get some intuition from the statistical model, we consider S_{AB} . For $\beta = AB$ in the noiseless case, the

dominant configuration is uniform with permutation \mathbb{C} throughout, yielding $F_{AB}^{(n,k)} = 0$ and hence $S_{AB} = 0$, consistent with the fact that the quantum state from the output of a noiseless circuit is a pure state.

C. Effects of quantum noise

We next describe how quantum noise modifies the effective statistical model. For concreteness, we illustrate the mapping using the reset quantum channel \mathcal{R} , though the resulting structure is independent of the specific choice of local noise channel.

In the replicated description, a reset channel modifies the weight of diagonal bonds connecting diagonally adjacent permutation spins:

$$\langle \sigma | \mathcal{R} | \tau \rangle = d^{r-|\tau|}. \quad (20)$$

This change propagates into the three-body triangle weights. For a downward triangle with identical spins, one finds

$$\begin{aligned} W^{\mathcal{R}}(\sigma, \sigma; \sigma) &= \sum_{\tau \in S_r} W_{g_{d^2}}^{(r)}(\sigma^{-1}\tau) d^{r-|\sigma^{-1}\tau|} d^{r-|\tau|} \\ &\sim d^{-|\sigma|}. \end{aligned} \quad (21)$$

Thus, quantum noise acts as a permutation *symmetry-breaking field* [118–125] that energetically favors the identity permutation \mathbb{I} . Because noise events occur at random space–time positions, they introduce *quenched disorder* into the classical spin model. Note that quantum noise also relaxes the unitary constraints [231, 232], i.e., $W^0(\mathbb{C}, \mathbb{C}; \mathbb{I}) = 0$ in the absence of quantum noise and thus this configuration is not allowed while $W^{\mathcal{R}}(\mathbb{C}, \mathbb{C}; \mathbb{I}) \sim d^{-|\mathbb{C}|}$ in the presence of quantum reset channel, and consequently enables additional spin configurations in the presence of noise [125].

In Sec. III B, we have shown that the dominant spin configuration for $\beta = AB$ in the absence of quantum noise is that all spins are \mathbb{C} . However, in the presence of quantum noise, this configuration acquires a weight proportional to $d^{-qLT|\mathbb{C}|}$ and is no longer energetically favored. See detailed discussion in Sec. IV for the favorable configurations in this case.

D. Effects of projective measurements

In the presence of projective measurements, the randomness of their space–time locations is likewise treated as quenched disorder. In the effective statistical model, as shown in Fig. 2, the corresponding diagonal bonds are removed when projective measurements are applied. Consequently, projective measurements act as a source of random Gaussian potentials and induce fluctuations of the domain wall away from its otherwise optimal trajectory [119].

Together, these ingredients constitute the statistical model description of noisy monitored circuits, enabling both analytical and numerical characterization of entanglement and information dynamics. Although the above discussion focuses on extracting entanglement-related observables (such as von Neumann entropy and mutual information) from the effective statistical model, the circuit-to-statistical-model mapping is more general. In particular, this framework has also been applied to study the dynamics of magic (nonstabilizer-ness) [137, 140] and random circuit sampling [180, 181] in noisy monitored circuits, revealing that the statistical description naturally extends beyond entanglement to other nonclassical resources in quantum many-body systems, including magic, fidelity, and cross-entropy benchmarking (XEB) [31, 233, 234].

IV. ENTANGLEMENT STRUCTURE OF STEADY STATES

A. KPZ scaling from fluctuating domain walls

In the presence of quantum noise, the entanglement structure of monitored circuits is qualitatively altered. Even an arbitrarily small noise rate $q > 0$ is sufficient to eliminate the volume-law phase entirely, thereby enforcing an entanglement area law for all values of the projective measurement probability [119–125]. Consequently, the conventional measurement-induced phase transition observed in noiseless circuits disappears. Nonetheless, the resulting noise-induced area law is far from trivial: the steady-state entanglement exhibits a universal and highly nontrivial dependence on the noise probability,

$$I_{A:B}(q) \sim q^{-1/3}, \quad (22)$$

where q is the quantum noise probability. Numerical results confirming this scaling are shown in Fig. 3. Below we outline how this behavior naturally emerges within the classical statistical-model description.

To develop an analytical understanding of the $q^{-1/3}$ scaling, we first examine how quantum noise modifies the dominant spin configurations in the associated statistical model. Noise events are treated as quenched disorder in space–time, and the dominant spin configuration is determined independently for each realization. As discussed in Sec. III C, the fully \mathbb{C} configuration that dominates $F_{AB}^{(n,k)}$ in the absence of noise becomes energetically disfavored once noise is introduced. Building on this observation, we now analyze how noise reshapes the dominant spin texture underlying the entanglement scaling.

As illustrated in Fig. 4(b), spins remain in \mathbb{C} until the backward-time propagation encounters a quantum noise $N(x_1, t_1)$ located at (x_1, t_1) ; all spins within the downward light-cone of this point flip from \mathbb{C} to \mathbb{I} , while all others remain unchanged. Subsequent quantum noises inside this region no longer affect the configuration since

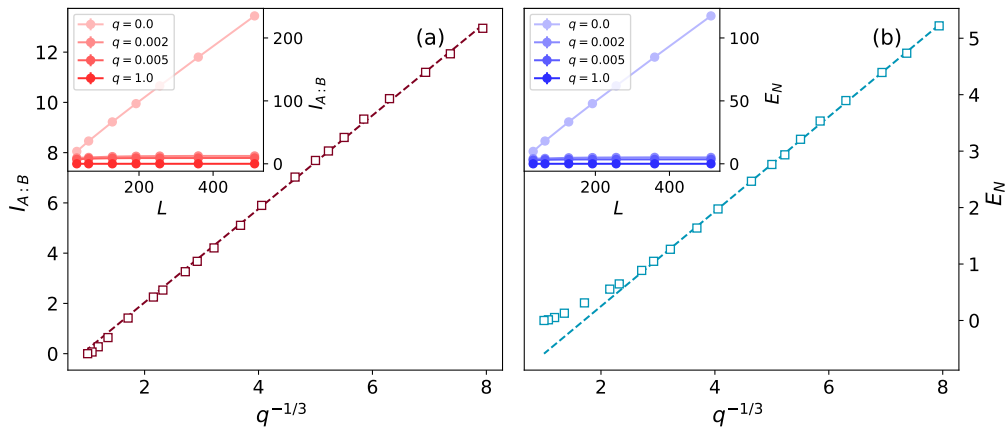


FIG. 3: $q^{-1/3}$ entanglement scaling in noisy monitored quantum circuits. (a) $I_{A:B}(q)$ and (b) $E_N(q)$ of the steady state of noisy monitored quantum circuits. The measurement probability is $p_m = 0.1 < p_m^c$. A characteristic $q^{-1/3}$ scaling emerges for the entanglement in the presence of noise. The insets show the dependence of $I_{A:B}$ and E_N on the system size L for various noise rates. Without noise, the entanglement exhibits a volume-law scaling since $p_m < p_m^c$, whereas any finite noise probability drives the system into an area-law regime. Reprinted with permission from Ref. [120], Copyright (2023) by the American Physical Society.

the spins around these noises are already \mathbb{I} . A noise event outside the light-cone, such as $N(x_2, t_2)$, generates its own backward light-cone, converting its interior spins from \mathbb{C} to \mathbb{I} . Thus, there is a domain wall separating \mathbb{C} and \mathbb{I} regions that is formed by the union of multiple light-cone boundaries, composed of many small segments. The typical distance of each small segment is governed by the mean spacing between noise events, yielding an effective length scale

$$L_{\text{eff}} \sim q^{-1}. \quad (23)$$

As illustrated in Fig. 4(a), the dominant spin configuration for $\beta = A$ or B can be interpreted in close analogy with that of $\beta = AB$. However, the distinct top boundary conditions imposed on A and B modify the local structure of the domain wall near the midpoint separating the two subsystems. In particular, this boundary constraint effectively reduces the characteristic length scale governing domain-wall fluctuations in this region. To leading order, the effective length scale is approximately halved, yielding an estimate of order $1/(2q)$ for the local domain-wall spacing.

Projective measurements act as a random Gaussian potential that perturbs the noise-determined domain-wall trajectory, inducing Kardar-Parisi-Zhang (KPZ) fluctuations [235–237] around the original light-cone path. A domain wall of characteristic scale q^{-1} therefore acquires a free-energy correction proportional to $q^{-1/3}$, in addition to its linear contribution. For the mutual information $I_{A:B} = S_A + S_B - S_{AB}$, bulk contributions cancel, leaving only the boundary free-energy cost near the midpoint between A and B . Because this boundary contribution inherits the KPZ fluctuation behavior, we obtain the universal scaling as the leading linear terms also cancel:

$$I_{A:B}(q) \sim q^{-1/3}, \quad (24)$$

which quantitatively characterizes the noise-induced area-law phase and demonstrates how quantum noise controls the steady-state entanglement structure.

B. Temporally correlated bulk noise

In the above discussion, we have established the $q^{-1/3}$ entanglement scaling in noisy monitored quantum circuits where noise events occur independently at random space-time locations. A natural question is whether temporal correlations between noise events can qualitatively alter this behavior. In the limit of strong temporal correlation, all noise events within a given trajectory share the same spatial locations across different discrete time steps, i.e., the spatial pattern of noises at every time slice is identical to that in the first time step shown in Fig. 1 (b).

The theoretical framework introduced in Sec. IV A can be naturally extended to the case of temporally correlated quantum noise. In this setting, correlated noise events act as emergent, extended boundaries in the statistical model, which in turn modify the dominant spin configuration and directly impose an effective length scale $L_{\text{eff}} \sim q^{-1}$ and thus the $q^{-1/3}$ entanglement scaling of the steady state remains.

C. Boundary noise

In addition to noisy monitored quantum circuits where quantum noises occur in the bulk, another important variant is the noisy monitored quantum circuit with quantum noises applied solely at the spatial boundaries [119]. In each discrete time step, quantum noise

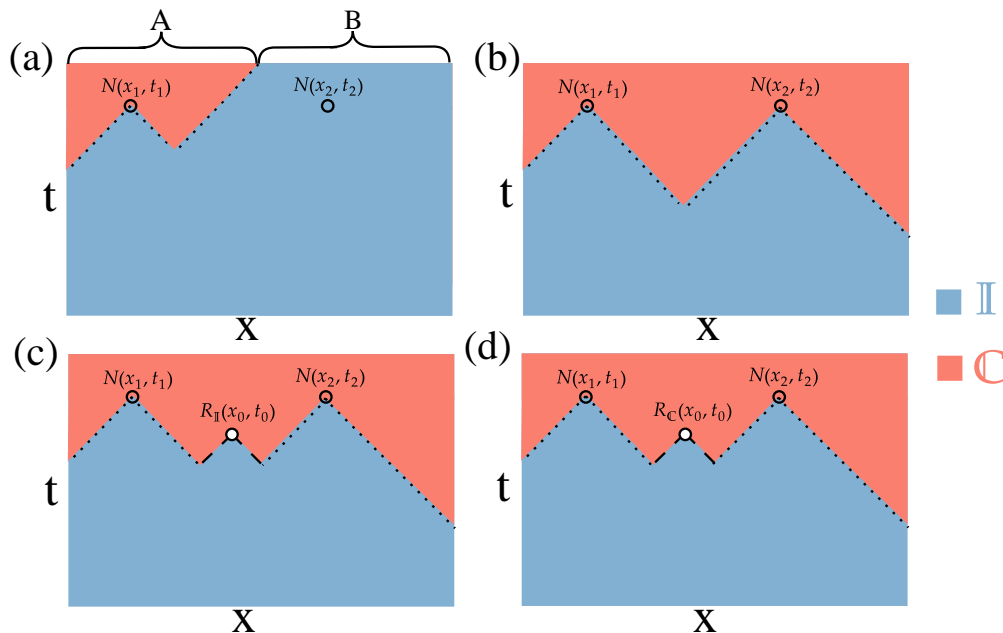


FIG. 4: *Statistical model understanding of entanglement structure and information protection timescale.* The schematic dominant spin configurations are illustrated here. The upper panel corresponds to the entanglement-generation setup, while the lower panel depicts the information-protection setup, where an additional Bell pair is introduced at (x_0, t_0) . The horizontal (x) and vertical (y) axes represent spatial and temporal directions, respectively. Different colors denote distinct permutation-spin configurations in the effective classical model. The symbols N and R mark the locations of quantum-noise events and the inserted Bell pair, respectively; for clarity, additional noise events inside the \mathbb{I} domain are omitted. Panel (a) shows the dominant configuration contributing to $F_A^{(n,k)}$. The presence of a midpoint defect on the top boundary modifies the local length scale of the adjacent domain-wall segment. Panel (b) depicts the dominant configuration relevant for $F_{AB}^{(n,k)}$. Panels (c) and (d) show the dominant configurations for $F_{AB}^{(n,k)}$ and $F_{AB \cup R}^{(n,k)}$, respectively, where the permutation spin at (x_0, t_0) is fixed to \mathbb{I} or \mathbb{C} depending on the boundary condition imposed by the Bell-pair encoding. In the presence of projective measurements, the domain wall exhibits fluctuations around its noise-determined trajectory. Reprinted with permission from Ref. [125], Copyright (2024) by the American Physical Society.

acts on the boundary sites, while projective measurements are still applied in the bulk, as illustrated in Fig. 5. This setup exhibits two notable features: (i) the quantum noises are strongly temporally correlated, and (ii) the effective noise occurrence probability scales as $O(1/L)$. This motivates, and is closely connected to, our later discussion of bulk noise models with system-size-dependent occurrence probability (see Sec. VI). In the boundary-noise case, $q \sim 1/L$, implying an effective length scale $L_{\text{eff}} \sim L$. Consequently, the entanglement exhibits KPZ-type scaling $L^{1/3}$, as shown in Fig. 5.

Throughout this discussion, the projective measurement probability is chosen such that $0 < p_m < p_m^c$ within the volume law phase, where p_m^c is the critical measurement probability for MIPT in the absence of quantum noise. The main results on entanglement scaling of the steady state in noisy monitored quantum circuits are summarized in Table. I.

V. INFORMATION PROTECTION TIMESCALE OF STEADY STATES

Although the entanglement scaling remains unchanged between temporally uncorrelated and temporally correlated quantum noises, the corresponding information-protection timescales differ markedly. Specifically, we discuss the information-protection capability of the steady state in the presence of quantum noise. To probe this property, one qudit of quantum information is encoded into the steady state by creating a Bell pair between a reference qudit and a system qudit, as illustrated in Fig. 1.

A. $q^{-2/3}$ scaling for temporally correlated noises and its relation with KPZ theory

The information-protection timescale for temporally correlated quantum noises can be naturally understood

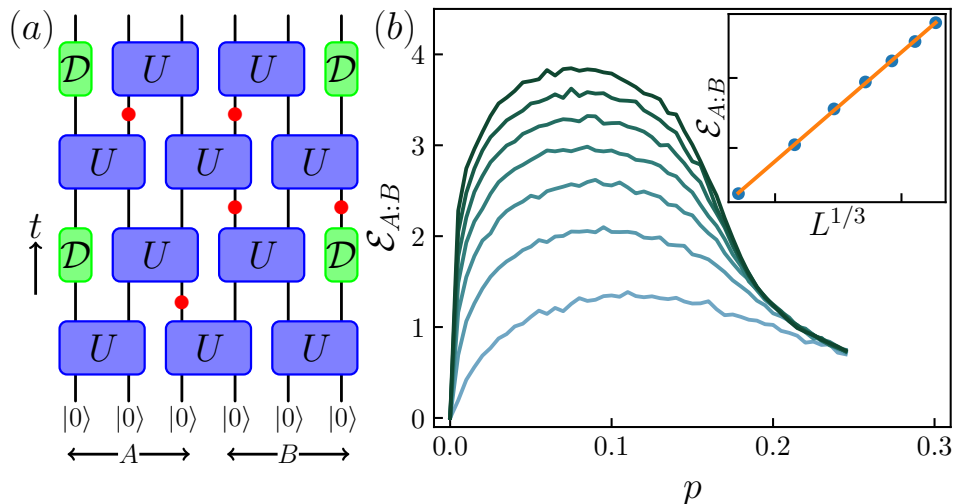


FIG. 5: *Measurement-induced KPZ entanglement scaling.* (a) Noisy monitored quantum circuits with quantum noise located at the boundary. (b) The entanglement for the steady state scales as $L^{1/3}$. Reprinted with permission from Ref. [119], Copyright (2022) by the American Physical Society.

TABLE I: Entanglement scaling in noisy monitored quantum circuits ($0 < p_m < p_m^c$)

	Entanglement scaling of the steady state
Temporally uncorrelated bulk noise	Area law, $q^{-1/3}$
Temporally correlated bulk noise	Area law, $q^{-1/3}$
Boundary noise	Power law, $L^{1/3}$

within the effective statistical-model description and is governed by KPZ-type domain-wall fluctuations. The dominant spin configurations contributing to $F_{AB}^{(n,k)}$, $F_R^{(n,k)}$, and $F_{ABUR}^{(n,k)}$ for $p_m = 0$ are illustrated in Fig. 7, where the top and bottom panels correspond to early- and late-time regimes, respectively. Throughout Fig. 7, we set $p_m = 0$; the inclusion of projective measurements ($0 < p_m < p_m^c$) merely induces fluctuations of the domain wall and modifies its vertical length scale, without altering the underlying analytical picture.

As shown in Fig. 7(b,e), the dominant spin configuration governing $F_R^{(n,k)}$ consists of all spins fixed to \mathbb{I} (blue region), except for the reference spin R , which is constrained to be \mathbb{C} (red circle). Consequently, S_R remains constant and receives contributions only from the localized “bubble” created by R_C .

In contrast, the dominant spin configurations contributing to $F_{AB}^{(n,k)}$ and $F_{ABUR}^{(n,k)}$ are modified once the reference spin R crosses the domain wall separating the \mathbb{C} (red region) and \mathbb{I} (blue region) domains. At this point, the mutual information $I_{AB:R}$ abruptly changes from 2 to 0, signaling a transition from perfect information protection to complete information loss. Accordingly, the information-protection timescale is determined by the average height of the domain wall—scaling as q^{-1} in the absence of projective measurements and as $q^{-2/3}$ when

monitored measurements induce KPZ-type fluctuations with wandering exponent $\chi = 2/3$. The numerical simulation has verified this analytical prediction, as shown in Fig. 6(b).

As discussed in Sec. IV C, boundary noise applied at fixed spatial boundaries can be regarded as a special case of temporally correlated bulk noise. In this situation, the effective length scale scales as $L_{\text{eff}} \sim L$, leading to a steady-state information-protection timescale of $O(L^{2/3})$. Another special case arises when quantum noise acts only at one single spatial boundary instead of both; see Sec. VIB for a detailed discussion.

Moreover, we note that this analytical understanding can be straightforwardly generalized to subsystem information protection in the steady state of conventional MITs. In this setting, instead of considering the mutual information $I_{AB:R}$ between the full system AB and a reference qudit R , we focus on the mutual information $I_{A:R}$, where A is a subsystem containing the system qudit that forms a Bell pair with the reference qudit during the encoding process. When the size of subsystem A is smaller than half of the total system, i.e., $L_A < L/2$, the remaining degrees of freedom can be regarded as an effective bath or environment. In this case, the statistical-model description is identical to that for temporally correlated noise. As illustrated in Fig. 8, once the reference spin R crosses the domain wall, the dominant spin configura-

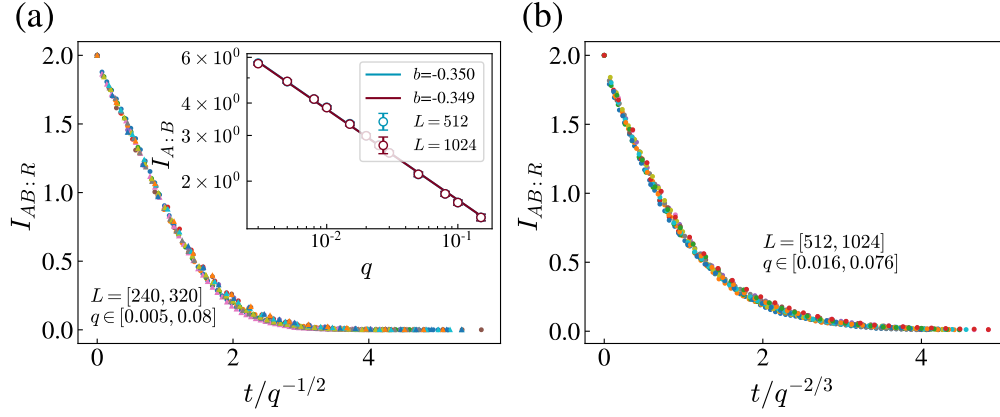


FIG. 6: *Information protection dynamics.* q represents the probability of reset channels and $p_m = 0.2 < p_m^c$ is the probability of projective measurement. (a) shows the mutual information $I_{AB:R}$ vs rescaled time $t/q^{-1/2}$ for temporally uncorrelated quantum noises. The inset shows the fitting of mutual information $I_{A:B}$ with the function $I_{A:B}(q) = aq^b$. b is very close to the theoretical prediction $-1/3$. (b) shows the mutual information $I_{AB:R}$ vs rescaled time $t/q^{-2/3}$ for temporally correlated quantum noises. Reprinted with permission from Ref. [125], Copyright (2024) by the American Physical Society.

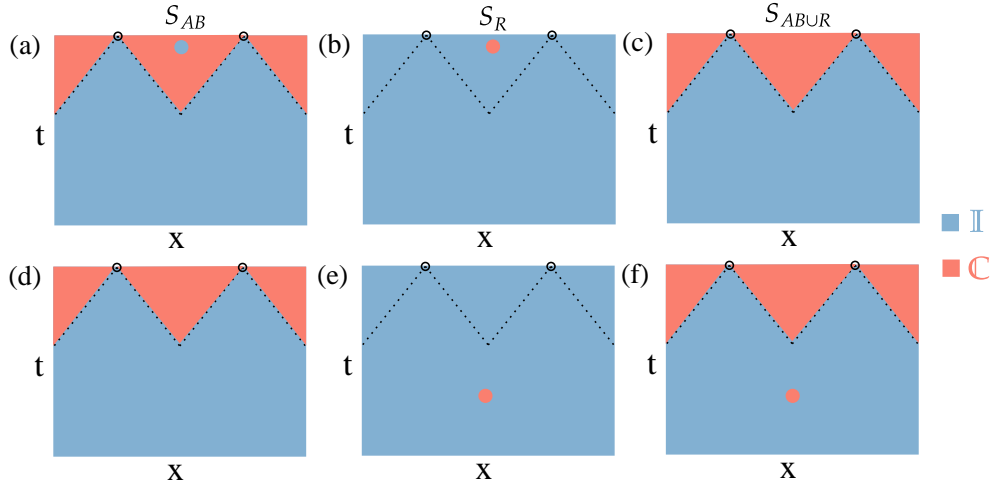


FIG. 7: *Statistical model understanding of information protection timescale for temporally correlated noise.* The top and bottom panels correspond to the early- and late-time regimes, respectively. For $F_{AB}^{(n,k)}$, the permutation spin associated with the reference qubit and the system qubit forming a Bell pair with it is fixed to \mathbb{I} , resulting in a localized “bubble” (blue circle) in panel (a). As the system evolves in time, this bubble effectively moves downward. Once it crosses the domain wall separating the \mathbb{C} and \mathbb{I} domains, the dominant spin configuration changes from (a) to (d). The similar analysis can also be applied to the dominant spin configuration for $F_{AB \cup R}^{(n,k)}$ as shown in (c) and (f). Consequently, the vertical length scale of the domain wall therefore sets the information-protection timescale.

tions governing $F_A^{(n,k)}$ and $F_{A \cup R}^{(n,k)}$ are altered, causing the mutual information to drop from 2 to 0. Consequently, the information-protection timescale is controlled by the vertical length scale of the domain wall and scales as $O(L_A)$ when $p_m = 0$, and as $O(L_A^{2/3})$ when $0 < p_m < p_m^c$ in the volume law phase.

B. $q^{-1/2}$ scaling for temporally uncorrelated noises and its relation with Hayden-Preskill protocol

However, for temporally uncorrelated noise, the information-protection timescale is no longer governed by the vertical domain-wall length scale. In the temporally correlated case, the reference qudit effectively moves downward in time without encountering additional noise events, and the dominant spin configuration changes only

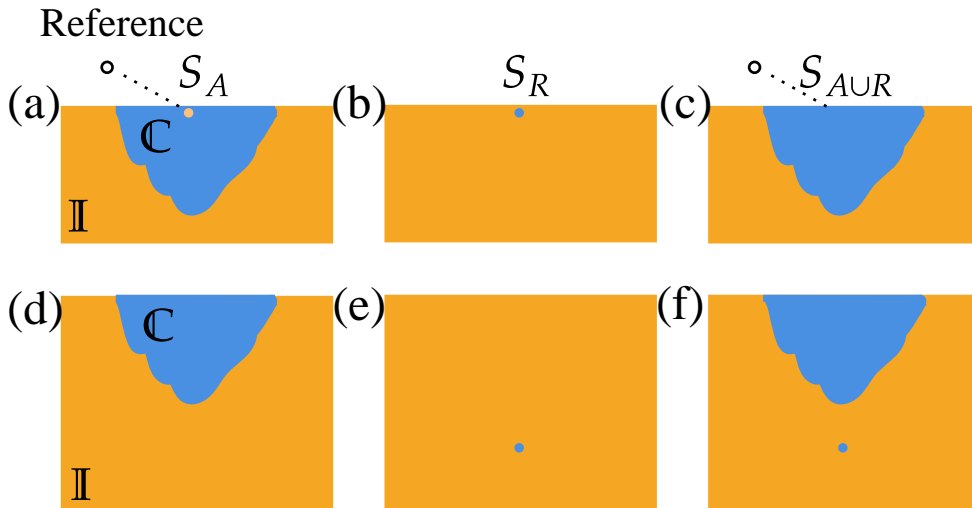


FIG. 8: *Statistical model understanding of the subsystem information-protection timescale of MITs.* Similar to the case with temporally correlated noise, the subsystem information-protection timescale is set by the vertical domain-wall length scale. Consequently, it scales as $O(L_A)$ for $p_m = 0$ and as $O(L_A^{2/3})$ for $0 < p_m < p_m^c$. Reprinted with permission from Ref. [125], Copyright (2024) by the American Physical Society.

when the reference qudit crosses the domain wall. By contrast, for temporally uncorrelated noise, the random space-time distribution of noise events allows the effectively moving reference qudit to encounter noise before reaching the domain wall, thereby altering the dominant spin configuration even before the original domain wall is crossed. See Fig. 4(c,d) for an alternative dominant spin configuration. At early time after encoding, where the reference space-time position plays a role similarly to a noise. For a longer time scale, when there are several noise events in the red region, they can form the new domain wall and leave the reference space-time position in the \mathbb{I} region.

This behavior can be understood more intuitively through the Hayden–Preskill protocol [238], schematically depicted in Fig. 9. Here the steady state plays the role of an old black hole maximally entangled with its environment (Bob). Alice encodes a one-qudit quantum message, maximally entangled with Charlie’s reference qudit, by injecting it into the black hole. Quantum noise channels function analogously to Hawking radiation emitted during the evaporation process. According to the Hayden–Preskill protocol, Bob needs only slightly more than one qudit of Hawking radiation to reconstruct Alice’s message. Consequently, the information-protection timescale is set by the time required for a noise event, occurring with probability q , to fall within the backward light-cone of area $O(t^2)$, leading to the scaling

$$t \sim q^{-1/2}. \quad (25)$$

The presence of projective measurements does not modify this qualitative understanding. Thus, the information-protection timescales for temporally uncorrelated quan-

tum noise scale as $q^{-1/2}$ for both $p_m = 0$ and $0 < p_m < p_m^c$.

Consequently, temporal correlations in the quantum noise lead to qualitatively distinct information-protection timescales in the steady state of noisy monitored circuits. In Sec. VIB, we turn to the complementary setting of initial-state encoding. The main results on the information protection timescales in noisy monitored quantum circuits are summarized in Table. II.

These intriguing dynamical phenomena including entanglement structure and information protection dynamics, uncovered in noisy monitored quantum circuits further motivate the study of novel quantum dynamics in broader classes of open quantum systems, such as monitored Hamiltonian systems with decoherence [73–77]. From an experimental perspective, these models provide compelling and accessible simulation tasks, potentially enabling the discovery of new nonequilibrium phases of matter.

However, in monitored systems, the intrinsic randomness of projective measurement outcomes gives rise to a severe post-selection problem [113–115], which poses a major challenge for experimental investigations of emergent phenomena. In particular, the probability of obtaining identical measurement trajectories required for measuring entanglement decreases exponentially with the number of measurements, leading to an exponentially large experimental cost. To address this challenge, several strategies have been proposed, including the use of cross-correlation [62], driven dynamics based on the Kibble–Zurek mechanism [64], and machine-learning-based approaches [239, 240]. These developments substantially mitigate the post-selection problem, making

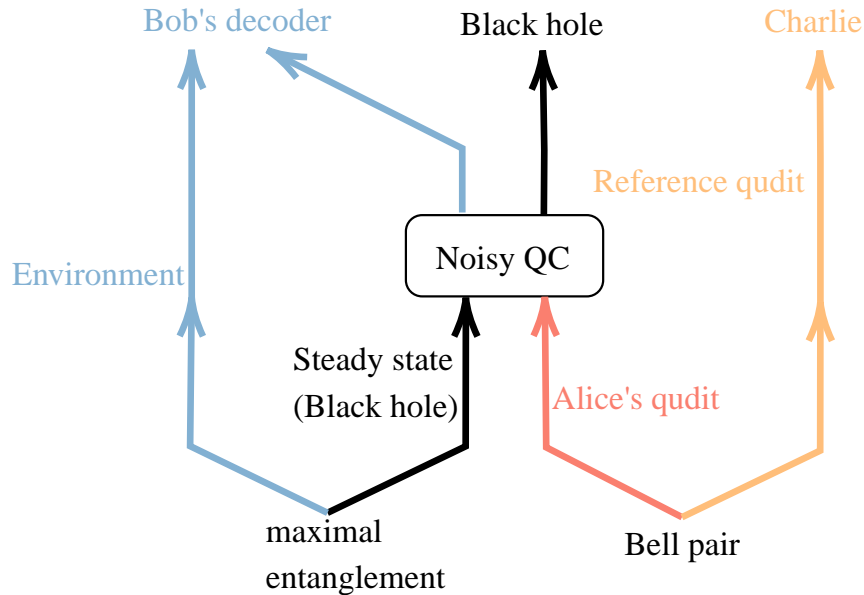


FIG. 9: *Connection between information protection in noisy quantum circuits and Hayden-Preskill protocol.* The steady state can be regarded as a black hole and Alice throws one-qudit information into the black hole to destroy it. The timescale of information protection corresponds to the time required for Bob to decode the information from collecting the qudits released by Hawking radiation. Reprinted with permission from Ref. [125], Copyright (2024) by the American Physical Society.

TABLE II: Information protection timescales with different settings ($0 < p_m < p_m^c$).

	Initial state (product state)	Steady state
Subsystem ($L_A < L/2$) without noise	$O(L_A)$	$O(L_A^{2/3})$
Whole system with temporally correlated noise	$O(q^{-1})$	$O(q^{-2/3})$
Whole system with temporally uncorrelated noise	$O(q^{-1})$	$O(q^{-1/2})$

the experimental exploration of novel phenomena in monitored systems increasingly feasible.

VI. NOISE-INDUCED PHASE TRANSITIONS

In the preceding discussion, the occurrence probability of quantum noise was assumed to be independent of the system size. We now consider a more general setting in which

$$q = \frac{p}{L^\alpha}, \quad (26)$$

where $\alpha = 0$ recovers the system-size-independent case analyzed above. In this broader framework, we discuss the resulting noise-induced phase transitions. We note that the setting involving boundary-localized noise [129] corresponds to a special case of this general framework with $\alpha = 1$.

A. Noise-induced entanglement phase transition

Although no entanglement phase transition occurs in the case $\alpha = 0$, this more general framework allows noise-induced phase transitions to emerge as p changes with $\alpha = 1$. We set $T = O(L)$, the same setting as that in normal MITPs.

Again, we first provide theoretical understanding from the statistical model. For the classical spin model associated with S_{AB} , the dominant configuration for $\alpha > 1$ is the fully aligned state in which all spins are fixed to \mathbb{C} , identical to the noiseless case. The free energy of this configuration scales as qLT , the average number of quantum-noise events, reflecting the magnetic-field-like pinning effect of the noise. In contrast, when $\alpha < 1$, the fully- \mathbb{C} configuration is no longer energetically favored. Instead, the configuration containing a domain wall, as discussed in Sec. IV A, has lower free energy, which scales as s_0L , where s_0 is a constant. Moreover, as discussed in Sec. IV A, the domain wall inherits an effective length scale $L_{\text{eff}} \sim q^{-1}$.

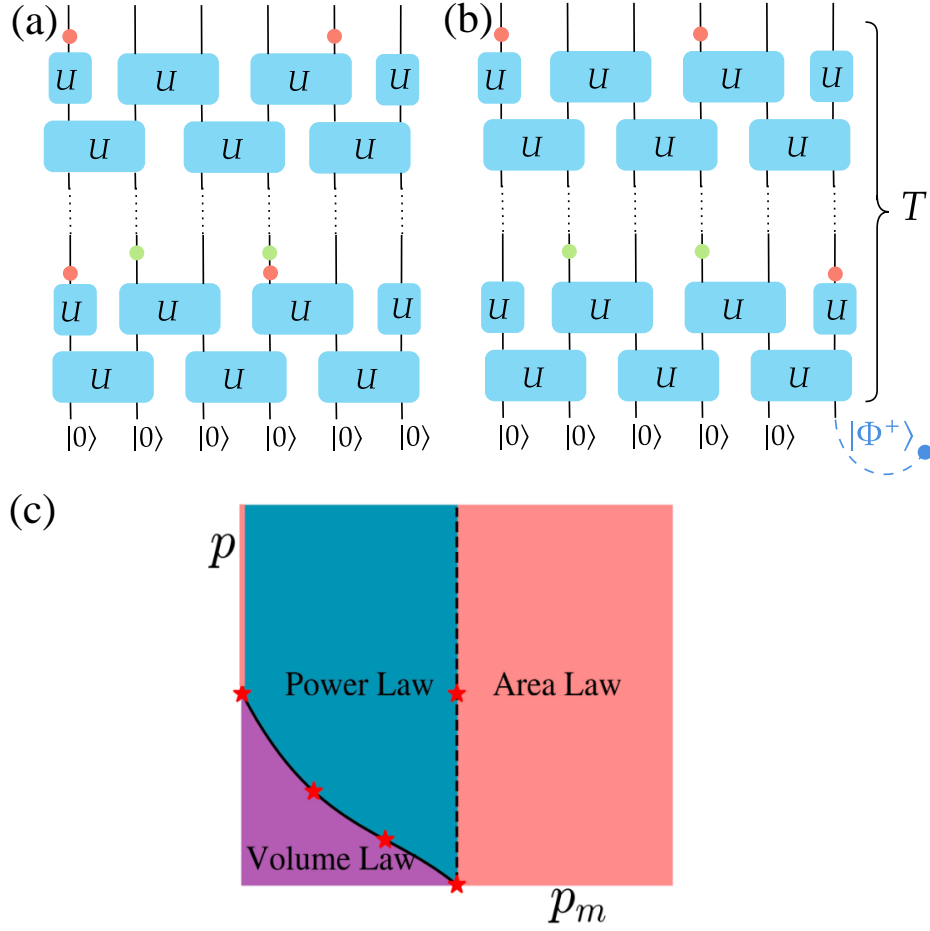


FIG. 10: *Setup and phase diagram for noise-induced entanglement and coding phase transitions.* Circuit setups with 6 qudits for (a) entanglement phase transition and (b) coding transition. The red and green circles represent the quantum channels and projective measurements, respectively. In (b), a qudit is maximally entangled with a reference qudit by creating a Bell pair $|\Phi^+\rangle$ to encode one qudit information. (c) Phase diagram of the entanglement phase transition with $T = 4L$. Red stars represent the critical points identified from numerical results. The black solid (dashed) curve denotes the noise (measurement)-induced phase transition. Reprinted with permission from Ref. [124], Copyright (2024) by the American Physical Society.

For the classical spin model corresponding to S_A or S_B , the domain-wall configuration is always energetically preferred due to the fixed top boundary condition. Consequently, when $\alpha = 1$, the system exhibits a competition between the two candidate configurations for S_{AB} . This leads to a volume-law entanglement phase when $p < s_0 L/T$, with mutual information scaling as $(s_0 - pT/L)L$, and an area-law phase when $p > s_0 L/T$. This crossover corresponds to the vertical transition line at $p_m = 0$ in Fig. 10(c).

Projective measurements do not modify the basic mechanism of the noise-induced transition—namely, the competition between the two spin configurations. However, they act as an attractive random Gaussian potential in the statistical model, causing the domain wall to fluctuate in such a way that it passes through more measurement events, thereby lowering its free energy. Following

Refs. [120, 125], the resulting domain-wall free energy acquires KPZ-type scaling, with a subleading correction proportional to $L_{\text{eff}}^{1/3} \sim L^{1/3}$ ($\alpha = 1$). Therefore, for $p > p_c$, the entanglement exhibits a power-law scaling $L^{1/3}$ in the presence of projective measurements, as indicated by the blue region in Fig. 10(c).

Importantly, this entanglement transition is a first-order transition arising from the competition between two distinct spin configurations. For $\alpha > 1$ ($\alpha < 1$), the fully-C configuration (the domain-wall configuration) always dominates, yielding a single volume-law (or power-law/area-law) phase. Thus, the noise-induced entanglement transition occurs only at the marginal point $\alpha = 1$.

B. Noise-induced coding transition

In Sec. V, we have discussed the information protection timescale of the steady state of the noisy monitored quantum circuits. In this section, we further discuss the information protection capacity of the initial state as well as the noise-induced coding transition.

We now extend the statistical-model framework to analyze the noise-induced coding transition. In addition to the top boundary conditions discussed previously, the spin at the bottom boundary, corresponding to the location where the Bell pair is introduced, is fixed by the boundary condition of the reference qudit: \mathbb{I} , \mathbb{C} , and \mathbb{C} for S_{AB} , S_R , and S_{ABUR} , respectively

For S_R , the dominant configuration features a bulk pinned to \mathbb{I} independently of the noise probability. Thus, S_R is constant, receiving only a unit contribution from the localized defect created by the Bell pair.

In contrast, for S_{AB} and S_{ABUR} , the competition persists between two distinct spin configurations: (i) the fully aligned configuration with all spins fixed to \mathbb{C} , and (ii) the configuration containing a topmost domain wall, similar to that discussed in Sec. VI A. When the former configuration dominates, the mutual information is $I_{AB:R} = 2$, indicating perfect protection of the encoded information. When the latter dominates, $I_{AB:R} = 0$, signaling complete loss of the encoded information. Thus, the encoded information remains perfectly protected below a critical value of the noise-strength prefactor p , and a noise-induced coding transition occurs as p increases. Within the unified statistical-model description, this coding transition is shown to share the same critical point and critical exponent as the noise-induced entanglement phase transition, which has been verified numerically as shown in Fig. 11. Moreover, in this initial-state encoding setup, temporal correlations between quantum noise events do not change the information-protection timescale, in contrast to the behavior in the steady-state encoding setup.

In Ref. [129], the noise-induced coding transition with quantum noise applied only at the left spatial boundary was investigated. The setup and corresponding phase diagram are shown in Fig. 12. This boundary-noise-induced coding transition differs qualitatively from the bulk-noise case. On the one hand, when the noise probability is below the critical value p_c , the encoded information is *perfectly* protected ($I_{AB:R} = 2$) in the presence of bulk noise, whereas it is only *partially* protected ($0 < I_{AB:R} < 2$) when the noise acts solely at the left boundary. On the other hand, for bulk noise the coding transition is always first order. In contrast, for boundary noise the transition is first order when $T/L > 1$, matching the behavior of the bulk case, but becomes continuous when $T/L < 1$. More detailed discussions can be found in Refs. [124, 129]. We note that the analytical understanding based on the effective statistical model in the large- d (local Hilbert space) limit does not qualitatively match numerical results obtained at finite d . This

discrepancy arises because, at finite d (finite temperature for statistical model), there is an additional entropic contribution to the free energy for the boundary noise case. This entropic effect plays a crucial role in the boundary-noise-induced coding transition at finite d . See Ref. [124] for a more detailed discussion.

Moreover, this initial state encoding and information protection scheme can also be extended to detect subsystem information protection where the complementary system is regarded as the environment. In such settings, the subsystem information protection measure is called the subsystem information capacity, which can be used to probe and characterize different dynamical phases [18, 241].

C. Noise-induced complexity transition

In addition to noise-induced entanglement and coding transitions, a noise-induced complexity phase transition in random circuit sampling has also been identified [180, 181] and experimentally demonstrated on a superconducting quantum processor [35]. The boundary between these phases can be resolved in finite-size systems using a fidelity-estimation technique known as cross-entropy benchmarking [31, 233, 234]. When the quantum noise is strong, the wavefunction effectively factorizes into multiple weakly correlated subsystems, and the circuit output can be efficiently spoofed by classical algorithms that simulate only a subset of the system. Conversely, when the noise is sufficiently weak, correlations extend across the entire circuit, restoring the intrinsic computational complexity required for quantum sampling. The phase diagram of this noise-induced complexity phase transition is shown in Fig. 13. We note that, similar to the noise-induced entanglement and coding transitions discussed above, this complexity transition also disappears when $\alpha \neq 1$.

D. Connections and Distinctions Between Noise-Induced Phase Transitions

In this section, we have introduced three types of noise-induced phase transitions: the noise-induced entanglement transition, coding transition, and complexity transition in random circuit sampling. All of these transitions occur when $\alpha = 1$ in the noise probability and disappear for other choices of α . From the perspective of the effective statistical model, the noise-induced entanglement and coding transitions share the same critical exponents and critical points that have been verified numerically. Moreover, their critical noise probabilities both depend on the ratio L/T and vanish in the limit $L/T \rightarrow 0$ even when $\alpha = 1$, consistent with the fact that any encoded information is ultimately destroyed in the presence of quantum noise.

In contrast, the noise-induced complexity transition in

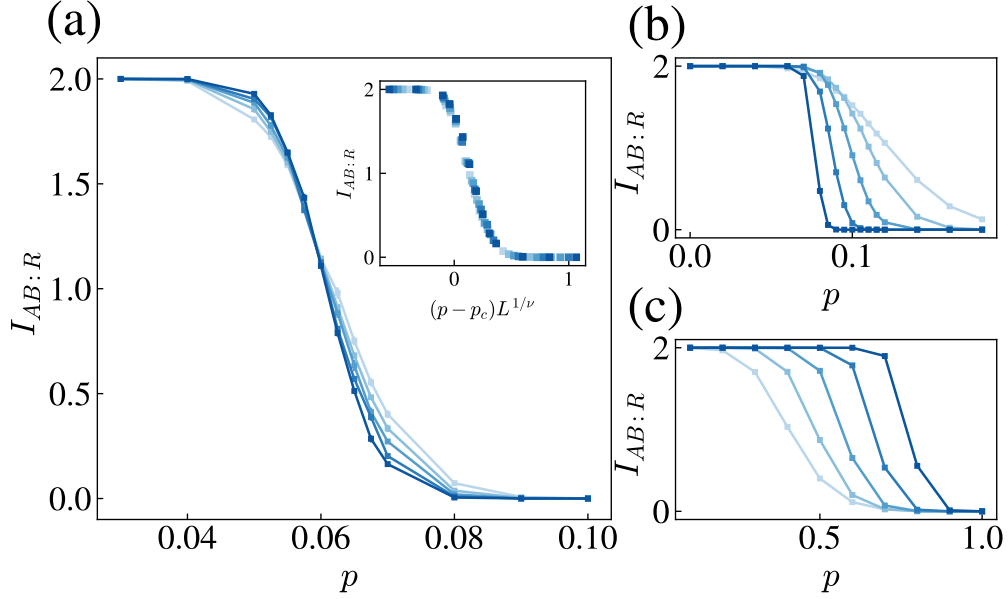


FIG. 11: *Numerical results of noise-induced coding transition.* (a) Quantum noise with $\alpha = 1$, $p_m = 0.2$, and $T = 4L$. Below p_c , the encoded information is perfectly protected. (b),(c) Mutual information $I_{AB:R}$ for $\alpha = 0.8$ and $\alpha = 1.2$, respectively. The noise-induced phase transition disappears in the thermodynamic limit when $\alpha \neq 1$. Reprinted with permission from Ref. [124], Copyright (2024) by the American Physical Society.

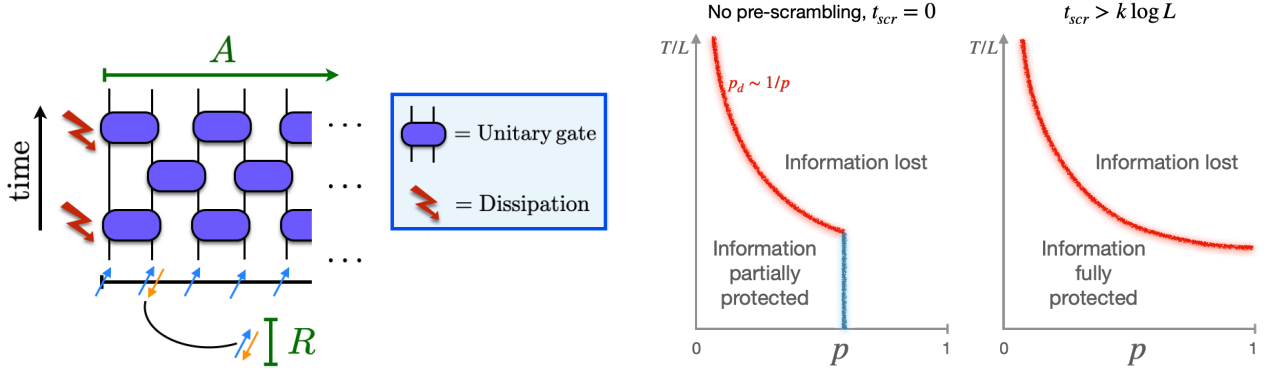


FIG. 12: *Setup and phase diagram of boundary noise-induced coding transition.* Left: schematic setup in which quantum noise is applied only at the left boundary. Right: phase diagram. Below the critical noise probability p_c , the encoded information is only *partially* protected, in contrast to the perfect protection in the case with bulk noise. Notably, when $T/L > 1$, the coding transition is first order (red line), whereas it becomes continuous when $T/L < 1$. With an additional pre-scrambling evolution, the encoded information can be perfectly protected. Reproduced from Ref. [129]. CC BY 4.0.

random circuit sampling [35, 180, 181], which is characterized by the linear cross-entropy benchmark rather than entanglement-based observables, exhibits a qualitatively different statistical-model structure. Only two replicas are involved in the statistical model analysis, and the critical noise probability p_c is independent of the ratio L/T , with analytical predictions yielding $p_c \approx 1$.

VII. BROADER APPLICATIONS OF NOISY QUANTUM CIRCUITS

Beyond their intrinsic theoretical interest, noisy quantum circuits have inspired a wide range of constructions and applications across quantum information science, quantum computation, and quantum many-body physics. One prominent example arises in the context of variational quantum algorithms, where noise-induced barren plateaus have been identified as a generic obstacle

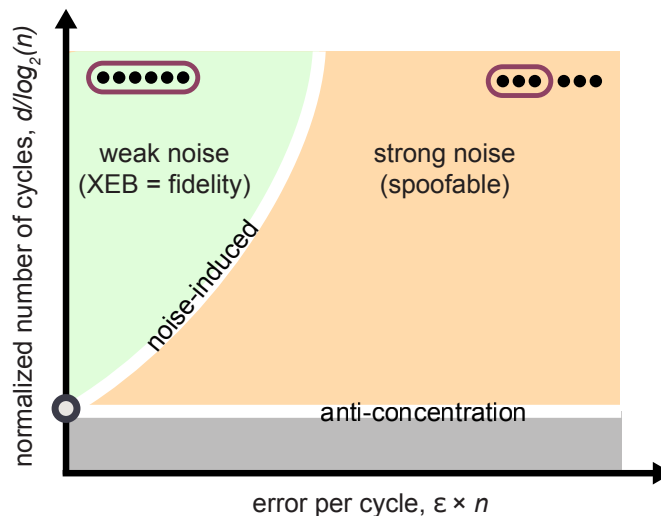


FIG. 13: *Noise-induced complexity transition in random circuit sampling*. In the weak-noise regime, the system is not classically simulable, whereas in the strong-noise regime it becomes classically simulable. Reproduced from Ref. [35]. [CC BY-NC-ND 4.0](#).

to trainability in the presence of decoherence [176, 177]. Interestingly, certain classes of noise, such as non-unital quantum channels or deliberately engineered dissipative mechanisms, can mitigate or even eliminate barren plateaus, thereby guiding the design of noise-resilient variational ansatzes [178, 179]. See Fig. 14 for the comparison of optimization landscapes in noisy quantum circuits. These findings highlight that noise, rather than being purely detrimental, can sometimes serve as a resource for optimization landscapes and variational quantum machine learning.

Noisy quantum circuits have also played a central role in sharpening our understanding of the boundary between classical simulability and genuine quantum advantage. While the computational cost of simulating noiseless RQCs grows exponentially, the introduction of noise can drastically alter their complexity. As discussed in Sec. VIC, there is a noise-induced complexity phase transition that separates a regime that remains classically intractable from one that becomes efficiently simulable [35, 180, 181]. This line of inquiry has additionally motivated the development of classical simulation techniques specifically tailored for noisy circuits, including unraveling-based trajectory methods [182–184] and Pauli-propagation or path-integral-inspired approaches [185–192]. These algorithms, many of which leverage the structure imposed by noise, have broadened the toolkit for understanding quantum dynamics in practical, imperfect settings.

From a quantum many-body perspective, noisy quantum circuits serve as a versatile platform for investigating mixed-state phases of matter. Recent studies have uncovered rich phenomena, including noise-induced ordering, dissipative phase transitions, and circuit-based characterizations of finite-temperature mixed states [193–196]. When noise respects certain symmetries, it can give rise

to unconventional phases such as strong-to-weak spontaneous symmetry breaking [197–207], which lack analogs in purely unitary limit.

Furthermore, profound connections have been established between noisy monitored quantum circuits and quantum error correction. Measurement-induced phase transitions have been shown to generate emergent quantum error-correcting structures [44, 45, 242], linking dynamical entanglement transitions to threshold phenomena in fault-tolerant quantum computation. Related developments include advances in quantum error mitigation [208–211] and new dissipative or measurement-assisted mechanisms for constructing quantum error-correcting codes [212–215]. Recently, topological order and symmetry-protected topological (SPT) phases have also been extensively investigated in noisy monitored quantum circuits [161, 164, 165, 170, 200, 243, 244]. The topological order or SPT phases are robust against local (symmetric) perturbations, whose intrinsic topological degeneracy or edge modes provide precisely the kind of redundancy required for encoding quantum information. This perspective highlights how noisy monitored quantum circuits can act as a resource for building and stabilizing error-correcting code spaces.

In sum, these works demonstrate that noisy monitored quantum circuits not only illuminate the fundamental behavior of quantum systems under decoherence, but also offer concrete guiding principles for engineering noise-resilient quantum technologies, including pathways toward measurement-assisted or dynamically stabilized quantum error correction.

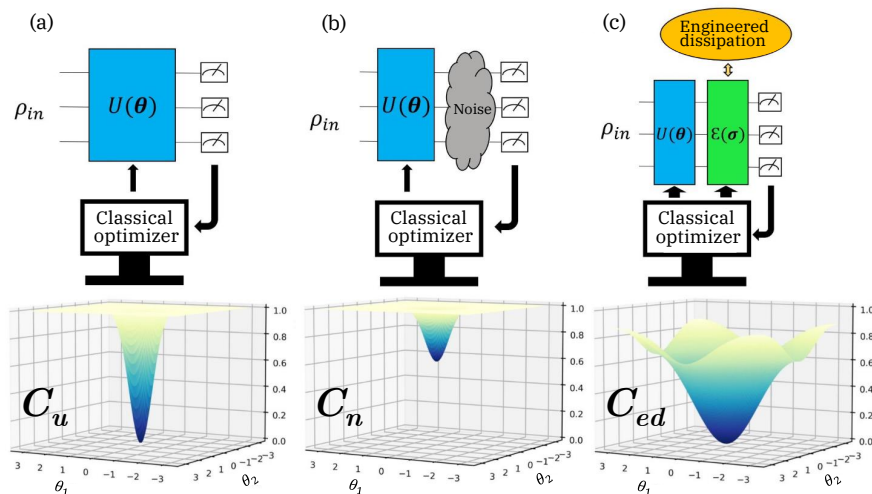


FIG. 14: *Comparison of optimization landscapes in noisy quantum circuits.* (a) fully unitary ansatz, (b) ansatz with depolarizing noise channels, (c) engineered-dissipation ansatz. The engineered-dissipation ansatz has the maximum variance and thus mitigate barren plateaus. Reproduced from Ref. [179]. **CC BY 4.0.**

VIII. DISCUSSIONS AND OUTLOOKS

In this review, we have presented a unified perspective on noisy monitored quantum circuits and their role at the interface of quantum information, quantum many-body physics, and quantum computation. By mapping circuit dynamics to classical statistical models in one higher dimension, we surveyed how quantum noise fundamentally reshapes entanglement structure, eliminates the conventional measurement-induced phase transition, and gives rise to universal scaling behaviors such as the characteristic $q^{-1/3}$ entanglement scaling. We further reviewed the information dynamics and information protection capabilities of noisy circuits, emphasizing the distinct timescales emerging from temporally uncorrelated and temporally correlated noise, and clarified their connections to domain-wall fluctuations and the Hayden–Preskill protocol. In addition, we discussed the broader landscape of noise-induced phase transitions, including the noise-induced entanglement, coding, complexity phase transitions.

Beyond these core results, we highlighted a wide array of applications inspired by noisy monitored circuits, ranging from new designs in variational quantum algorithms and new classical simulation techniques to mixed-state phases of matter and developments in quantum error mitigation and correction. These directions demonstrate that noisy circuits are not merely a theoretical abstraction, but a practical framework for understanding and harnessing the interplay between randomness, measurement, and decoherence.

Looking ahead, several promising avenues merit further exploration. First, extending the statistical-model framework to quantum noise with tunable correlation strength, and higher-dimensional architectures may reveal new universality classes and dynamical phases. Sec-

ond, the information-theoretic viewpoint suggests deeper connections between noisy circuit dynamics, black-hole-inspired decoding protocols, and fault-tolerant quantum computation. Third, the growing experimental capabilities of superconducting qubits [114, 115, 161], trapped ions [113], and Rydberg arrays [245–258] provide an exciting opportunity to probe noise-induced phenomena in regimes inaccessible to classical simulation. Finally, the interplay between noise and structure, such as symmetry, topology, long-range interactions, or tailored dissipative mechanisms, may enable the design of new dynamical phases, noise-resilient algorithms, and emergent error-correcting patterns.

Taken together, these developments position noisy monitored quantum circuits as a powerful and versatile platform for uncovering universal features of quantum dynamics in realistic, decohering environments, and for guiding the next generation of quantum technologies.

IX. ACKNOWLEDGEMENT

SXZ acknowledges the support from Innovation Program for Quantum Science and Technology (2024ZD0301700) and the National Natural Science Foundation of China (No. 12574546). SL’s work at Princeton University was supported by the Gordon and Betty Moore Foundation through Grant No. GBMF8685 toward the Princeton theory program, the Gordon and Betty Moore Foundations EPiQS Initiative (Grant No. GBMF11070), the Office of Naval Research (ONR Grant No. N00014-20-1-2303), the Global Collaborative Network Grant at Princeton University, the Simons Investigator Grant No. 404513, the BSF Israel US foundation No. 2018226, the NSF-MERSEC (Grant No. MERSEC DMR 2011750), the Simons Collaboration on

New Frontiers in Superconductivity, and the Schmidt Foundation at the Princeton University. The work

of S.- K.J. is supported by a start-up fund at Tulane University.

-
- [1] M. P. Fisher, V. Khemani, A. Nahum, and S. Vijay, Random quantum circuits, *Annual Review of Condensed Matter Physics* **14**, 335 (2023).
- [2] A. Chandran and C. R. Laumann, Semiclassical limit for the many-body localization transition, *Phys. Rev. B* **92**, 024301 (2015).
- [3] A. Nahum, J. Ruhman, S. Vijay, and J. Haah, Quantum entanglement growth under random unitary dynamics, *Phys. Rev. X* **7**, 031016 (2017).
- [4] A. Nahum, S. Vijay, and J. Haah, Operator spreading in random unitary circuits, *Phys. Rev. X* **8**, 021014 (2018).
- [5] T. Rakovszky, F. Pollmann, and C. W. von Keyserlingk, Diffusive hydrodynamics of out-of-time-ordered correlators with charge conservation, *Phys. Rev. X* **8**, 031058 (2018).
- [6] B. Bertini, P. Kos, and T. c. v. Prosen, Exact spectral form factor in a minimal model of many-body quantum chaos, *Phys. Rev. Lett.* **121**, 264101 (2018).
- [7] C. W. von Keyserlingk, T. Rakovszky, F. Pollmann, and S. L. Sondhi, Operator hydrodynamics, otocs, and entanglement growth in systems without conservation laws, *Phys. Rev. X* **8**, 021013 (2018).
- [8] V. Khemani, A. Vishwanath, and D. A. Huse, Operator spreading and the emergence of dissipative hydrodynamics under unitary evolution with conservation laws, *Phys. Rev. X* **8**, 031057 (2018).
- [9] T. Zhou and A. Nahum, Emergent statistical mechanics of entanglement in random unitary circuits, *Phys. Rev. B* **99**, 174205 (2019).
- [10] S. Gopalakrishnan and A. Lamacraft, Unitary circuits of finite depth and infinite width from quantum channels, *Phys. Rev. B* **100**, 064309 (2019).
- [11] B. Bertini, P. Kos, and T. c. v. Prosen, Exact correlation functions for dual-unitary lattice models in 1 + 1 dimensions, *Phys. Rev. Lett.* **123**, 210601 (2019).
- [12] T. Zhou and A. Nahum, Entanglement membrane in chaotic many-body systems, *Phys. Rev. X* **10**, 031066 (2020).
- [13] P. Kos, B. Bertini, and T. c. v. Prosen, Correlations in perturbed dual-unitary circuits: Efficient path-integral formula, *Phys. Rev. X* **11**, 011022 (2021).
- [14] A. Foligno, T. Zhou, and B. Bertini, Temporal entanglement in chaotic quantum circuits, *Phys. Rev. X* **13**, 041008 (2023).
- [15] S. Liu, H.-K. Zhang, S. Yin, and S.-X. Zhang, Symmetry restoration and quantum mpemba effect in symmetric random circuits, *Phys. Rev. Lett.* **133**, 140405 (2024).
- [16] X. Turkeshi, P. Calabrese, and A. De Luca, Quantum mpemba effect in random circuits, *Phys. Rev. Lett.* **135**, 040403 (2025).
- [17] A. Foligno, P. Calabrese, and B. Bertini, Nonequilibrium dynamics of charged dual-unitary circuits, *PRX Quantum* **6**, 010324 (2025).
- [18] Y.-Q. Chen, S. Liu, and S.-X. Zhang, Subsystem Information Capacity in Random Circuits and Hamiltonian Dynamics, *Quantum* **9**, 1783 (2025).
- [19] F. Ares, S. Murciano, P. Calabrese, and L. Piroli, Entanglement asymmetry dynamics in random quantum circuits, *Phys. Rev. Res.* **7**, 033135 (2025).
- [20] H.-Z. Li, C. H. Lee, S. Liu, S.-X. Zhang, and J.-X. Zhong, Quantum mpemba effect in long-ranged $u(1)$ -symmetric random circuits, [arXiv:2512.06775](https://arxiv.org/abs/2512.06775) (2025).
- [21] C.-Y. Zhang, Z.-X. Li, and S.-X. Zhang, Entanglement growth from entangled states: A unified perspective on entanglement generation and transport, [arXiv:2510.08344](https://arxiv.org/abs/2510.08344) (2025).
- [22] Z. Li, H. Zheng, J. Liu, L. Jiang, and Z.-W. Liu, Designs from local random quantum circuits with $SU(d)$ symmetry, *PRX Quantum* **5**, 040349 (2024).
- [23] Z. Li, H. Zheng, and Z.-W. Liu, Efficient quantum pseudorandomness under conservation laws, [arXiv:2411.04893](https://arxiv.org/abs/2411.04893) (2024).
- [24] T. Schuster, J. Haferkamp, and H.-Y. Huang, Random unitaries in extremely low depth, *Science* **389**, 92 (2025).
- [25] T. Schuster, F. Ma, A. Lombardi, F. Brandao, and H.-Y. Huang, Strong random unitaries and fast scrambling, [arXiv:2509.26310](https://arxiv.org/abs/2509.26310) (2025).
- [26] L. Cui, T. Schuster, F. Brandao, and H.-Y. Huang, Unitary designs in nearly optimal depth, [arXiv:2507.06216](https://arxiv.org/abs/2507.06216) (2025).
- [27] B. Foxman, N. Parham, F. Vasconcelos, and H. Yuen, Random unitaries in constant (quantum) time, [arXiv:2508.11487](https://arxiv.org/abs/2508.11487) (2025).
- [28] L. Mao, L. Cui, T. Schuster, and H.-Y. Huang, Random unitaries that conserve energy, [arXiv:2510.08448](https://arxiv.org/abs/2510.08448) (2025).
- [29] Z. Li, H. Zheng, Y. Wang, L. Jiang, Z.-W. Liu, and J. Liu, $SU(d)$ -symmetric random unitaries: quantum scrambling, error correction, and machine learning, *npj Quantum Information* **11**, 158 (2025).
- [30] Y. Zhang, S. Vijay, Y. Gu, and Y. Bao, Designs from magic-augmented clifford circuits, [arXiv:2507.02828](https://arxiv.org/abs/2507.02828) (2025).
- [31] F. Arute, K. Arya, R. Babbush, D. Bacon, J. C. Bardin, R. Barends, R. Biswas, S. Boixo, F. G. S. L. Brandao, D. A. Buell, B. Burkett, Y. Chen, Z. Chen, B. Chiaro, R. Collins, W. Courtney, A. Dunsworth, E. Farhi, B. Foxen, A. Fowler, C. Gidney, M. Giustina, R. Graff, K. Guerin, S. Habegger, M. P. Harrigan, M. J. Hartmann, A. Ho, M. Hoffmann, T. Huang, T. S. Humble, S. V. Isakov, E. Jeffrey, Z. Jiang, D. Kafri, K. Kechedzhi, J. Kelly, P. V. Klimov, S. Knysh, A. Korotkov, F. Kostritsa, D. Landhuis, M. Lindmark, E. Lucero, D. Lyakh, S. Mandrà, J. R. McClean, M. McEwen, A. Megrant, X. Mi, K. Michielsen, M. Mohseni, J. Mutus, O. Naaman, M. Neeley, C. Neill, M. Y. Niu, E. Ostby, A. Petukhov, J. C. Platt, C. Quintana, E. G. Rieffel, P. Roushan, N. C. Rubin, D. Sank, K. J. Satzinger, V. Smelyanskiy, K. J. Sung, M. D. Trevithick, A. Vainsencher, B. Villalonga, T. White, Z. J. Yao, P. Yeh, A. Zalcman, H. Neven, and J. M. Martinis, Quantum supremacy using a programmable supercon-

- ducting processor, *Nature* **574**, 505 (2019).
- [32] M.-C. Chen, R. Li, L. Gan, X. Zhu, G. Yang, C.-Y. Lu, and J.-W. Pan, Quantum-teleportation-inspired algorithm for sampling large random quantum circuits, *Phys. Rev. Lett.* **124**, 080502 (2020).
- [33] Y. Wu, W.-S. Bao, S. Cao, F. Chen, M.-C. Chen, X. Chen, T.-H. Chung, H. Deng, Y. Du, D. Fan, M. Gong, C. Guo, C. Guo, S. Guo, L. Han, L. Hong, H.-L. Huang, Y.-H. Huo, L. Li, N. Li, S. Li, Y. Li, F. Liang, C. Lin, J. Lin, H. Qian, D. Qiao, H. Rong, H. Su, L. Sun, L. Wang, S. Wang, D. Wu, Y. Xu, K. Yan, W. Yang, Y. Yang, Y. Ye, J. Yin, C. Ying, J. Yu, C. Zha, C. Zhang, H. Zhang, K. Zhang, Y. Zhang, H. Zhao, Y. Zhao, L. Zhou, Q. Zhu, C.-Y. Lu, C.-Z. Peng, X. Zhu, and J.-W. Pan, Strong quantum computational advantage using a superconducting quantum processor, *Phys. Rev. Lett.* **127**, 180501 (2021).
- [34] Q. Zhu, S. Cao, F. Chen, M.-C. Chen, X. Chen, T.-H. Chung, H. Deng, Y. Du, D. Fan, M. Gong, C. Guo, C. Guo, S. Guo, L. Han, L. Hong, H.-L. Huang, Y.-H. Huo, L. Li, N. Li, S. Li, Y. Li, F. Liang, C. Lin, J. Lin, H. Qian, D. Qiao, H. Rong, H. Su, L. Sun, L. Wang, S. Wang, D. Wu, Y. Wu, Y. Xu, K. Yan, W. Yang, Y. Yang, Y. Ye, J. Yin, C. Ying, J. Yu, C. Zha, C. Zhang, H. Zhang, K. Zhang, Y. Zhang, H. Zhao, Y. Zhao, L. Zhou, C.-Y. Lu, C.-Z. Peng, X. Zhu, and J.-W. Pan, Quantum computational advantage via 60-qubit 24-cycle random circuit sampling, *Science Bulletin* **67**, 240 (2022).
- [35] A. Morvan, B. Villalonga, X. Mi, S. Mandr a, A. Bengtsson, P. V. Klimov, Z. Chen, S. Hong, C. Erickson, I. K. Drozdov, J. Chau, G. Laun, R. Movassagh, A. Asfah, L. T. A. N. Brand o, R. Peralta, D. Abanin, R. Acharya, R. Allen, T. I. Andersen, K. Anderson, M. Ansmann, F. Arute, K. Arya, J. Atalaya, J. C. Bardin, A. Bilmes, G. Bortoli, A. Bourassa, J. Bovaird, L. Brill, M. Broughton, B. B. Buckley, D. A. Buell, T. Burger, B. Burkett, N. Bushnell, J. Campero, H.-S. Chang, B. Chiaro, D. Chik, C. Chou, J. Coogan, R. Collins, P. Conner, W. Courtney, A. L. Crook, B. Curtin, D. M. Debroy, A. D. T. Barba, S. Demura, A. D. Paolo, A. Dunsworth, L. Faoro, E. Farhi, R. Fatemi, V. S. Ferreira, L. F. Burgos, E. Forati, A. G. Fowler, B. Foxen, G. Garcia,  . Genois, W. Giang, C. Gidney, D. Gilboa, M. Giustina, R. Gosula, A. G. Dau, J. A. Gross, S. Habegger, M. C. Hamilton, M. Hansen, M. P. Harrigan, S. D. Harrington, P. Heu, M. R. Hoffmann, T. Huang, A. Huff, W. J. Huggins, L. B. Ioffe, S. V. Isakov, J. Iveland, E. Jeffrey, Z. Jiang, C. Jones, P. Juhas, D. Kafri, T. Khattar, M. Khezri, M. Kieferov a, S. Kim, A. Kitaev, A. R. Klots, A. N. Korotkov, F. Kostritsa, J. M. Kreikebaum, D. Landhuis, P. Laptev, K.-M. Lau, L. Laws, J. Lee, K. W. Lee, Y. D. Lensky, B. J. Lester, A. T. Lill, W. Liu, W. P. Livingston, A. Locharla, F. D. Malone, O. Martin, S. Martin, J. R. McClean, M. McEwen, K. C. Miao, A. Mieszala, S. Montazeri, W. Mroczkiewicz, O. Naaman, M. Neeley, C. Neill, A. Nersisyan, M. Newman, J. H. Ng, A. Nguyen, M. Nguyen, M. Y. Niu, T. E. O Brien, S. Omonije, A. Opremcak, A. Petukhov, R. Potter, L. P. Pryadko, C. Quintana, D. M. Rhodes, C. Rocque, E. Rosenberg, N. C. Rubin, N. Saei, D. Sank, K. Sankaragomathi, K. J. Satzinger, H. F. Schurkus, C. Schuster, M. J. Shearn, A. Shorter, N. Shu y, V. Shvarts, V. Sivak, J. Skrzynny, W. C. Smith, R. D. Somma, G. Sterling, D. Strain, M. Szalay, D. Thor, A. Torres, G. Vidal, C. V. Heidweiller, T. White, B. W. K. Woo, C. Xing, Z. J. Yao, P. Yeh, J. Yoo, G. Young, A. Zalcman, Y. Zhang, N. Zhu, N. Zobrist, E. G. Rieffel, R. Biswas, R. Babbush, D. Bacon, J. Hilton, E. Lucero, H. Neven, A. Megrant, J. Kelly, P. Roushan, I. Aleiner, V. Smelyanskiy, K. Kechedzhi, Y. Chen, and S. Boixo, Phase transitions in random circuit sampling, *Nature* **634**, 328 (2024).
- [36] H.-Y. Huang, R. Kueng, and J. Preskill, Predicting many properties of a quantum system from very few measurements, *Nature Physics* **16**, 1050 (2020).
- [37] A. Elben, S. T. Flammia, H.-Y. Huang, R. Kueng, J. Preskill, B. Vermersch, and P. Zoller, The randomized measurement toolbox, *Nature Reviews Physics* **5**, 9 (2023).
- [38] M. Cerezo, A. Arrasmith, R. Babbush, S. C. Benjamin, S. Endo, K. Fujii, J. R. McClean, K. Mitarai, X. Yuan, L. Cincio, and P. J. Coles, Variational quantum algorithms, *Nature Reviews Physics* **3**, 625 (2021).
- [39] K. Bharti, A. Cervera-Lierta, T. H. Kyaw, T. Haug, S. Alperin-Lea, A. Anand, M. Degroote, H. Heimonen, J. S. Kottmann, T. Menke, W.-K. Mok, S. Sim, L.-C. Kwek, and A. Aspuru-Guzik, Noisy intermediate-scale quantum algorithms, *Rev. Mod. Phys.* **94**, 015004 (2022).
- [40] Y. Li, X. Chen, and M. P. A. Fisher, Quantum zeno effect and the many-body entanglement transition, *Phys. Rev. B* **98**, 205136 (2018).
- [41] Y. Li, X. Chen, and M. P. A. Fisher, Measurement-driven entanglement transition in hybrid quantum circuits, *Phys. Rev. B* **100**, 134306 (2019).
- [42] B. Skinner, J. Ruhman, and A. Nahum, Measurement-induced phase transitions in the dynamics of entanglement, *Phys. Rev. X* **9**, 031009 (2019).
- [43] A. Chan, R. M. Nandkishore, M. Pretko, and G. Smith, Unitary-projective entanglement dynamics, *Phys. Rev. B* **99**, 224307 (2019).
- [44] M. J. Gullans and D. A. Huse, Dynamical purification phase transition induced by quantum measurements, *Phys. Rev. X* **10**, 041020 (2020).
- [45] S. Choi, Y. Bao, X.-L. Qi, and E. Altman, Quantum error correction in scrambling dynamics and measurement-induced phase transition, *Phys. Rev. Lett.* **125**, 030505 (2020).
- [46] Y. Bao, S. Choi, and E. Altman, Theory of the phase transition in random unitary circuits with measurements, *Phys. Rev. B* **101**, 104301 (2020).
- [47] C.-M. Jian, Y.-Z. You, R. Vasseur, and A. W. W. Ludwig, Measurement-induced criticality in random quantum circuits, *Phys. Rev. B* **101**, 104302 (2020).
- [48] X. Turkeshi, R. Fazio, and M. Dalmonte, Measurement-induced criticality in $(2 + 1)$ -dimensional hybrid quantum circuits, *Phys. Rev. B* **102**, 014315 (2020).
- [49] A. Zabalo, M. J. Gullans, J. H. Wilson, S. Gopalakrishnan, D. A. Huse, and J. H. Pixley, Critical properties of the measurement-induced transition in random quantum circuits, *Phys. Rev. B* **101**, 060301 (2020).
- [50] J. Iaconis, A. Lucas, and X. Chen, Measurement-induced phase transitions in quantum automaton circuits, *Phys. Rev. B* **102**, 224311 (2020).
- [51] M. J. Gullans and D. A. Huse, Scalable probes of measurement-induced criticality, *Phys. Rev. Lett.* **125**,

- 070606 (2020).
- [52] M. Ippoliti and V. Khemani, Postselection-free entanglement dynamics via spacetime duality, *Phys. Rev. Lett.* **126**, 060501 (2021).
- [53] T.-C. Lu and T. Grover, Spacetime duality between localization transitions and measurement-induced transitions, *PRX Quantum* **2**, 040319 (2021).
- [54] R. Fan, S. Vijay, A. Vishwanath, and Y.-Z. You, Self-organized error correction in random unitary circuits with measurement, *Phys. Rev. B* **103**, 174309 (2021).
- [55] Y. Li and M. P. A. Fisher, Statistical mechanics of quantum error correcting codes, *Phys. Rev. B* **103**, 104306 (2021).
- [56] M. Ippoliti, T. Rakovszky, and V. Khemani, Fractal, logarithmic, and volume-law entangled nonthermal steady states via spacetime duality, *Phys. Rev. X* **12**, 011045 (2022).
- [57] Z.-C. Yang, Y. Li, M. P. A. Fisher, and X. Chen, Entanglement phase transitions in random stabilizer tensor networks, *Phys. Rev. B* **105**, 104306 (2022).
- [58] P. Sierant, M. Schirò, M. Lewenstein, and X. Turkeshi, Measurement-induced phase transitions in $(d + 1)$ -dimensional stabilizer circuits, *Phys. Rev. B* **106**, 214316 (2022).
- [59] H. Liu, T. Zhou, and X. Chen, Measurement-induced entanglement transition in a two-dimensional shallow circuit, *Phys. Rev. B* **106**, 144311 (2022).
- [60] Q. Zhang and G.-M. Zhang, Noise-induced entanglement transition in one-dimensional random quantum circuits, *Chinese Physics Letters* **39**, 050302 (2022).
- [61] Y. Han and X. Chen, Entanglement dynamics in U(1) symmetric hybrid quantum automaton circuits, *Quantum* **7**, 1200 (2023).
- [62] S. J. Garratt and E. Altman, Probing postmeasurement entanglement without postselection, *PRX Quantum* **5**, 030311 (2024).
- [63] A. A. Akhtar, H.-Y. Hu, and Y.-Z. You, Measurement-induced criticality is tomographically optimal, *Phys. Rev. B* **109**, 094209 (2024).
- [64] W. Wang, S. Liu, J. Li, S.-X. Zhang, and S. Yin, Driven critical dynamics in measurement-induced phase transitions, *arXiv:2411.06648* (2024).
- [65] G. M. Sommers, S. Gopalakrishnan, M. J. Gullans, and D. A. Huse, Zero-temperature entanglement membranes in quantum circuits, *Phys. Rev. B* **110**, 064311 (2024).
- [66] S. P. Kelly and J. Marino, Entanglement transitions induced by quantum-data collection, *Phys. Rev. A* **111**, L010402 (2025).
- [67] S. P. Kelly and J. Marino, Generalizing measurement-induced phase transitions to information exchange symmetry breaking, *Phys. Rev. A* **111**, 012425 (2025).
- [68] W. Wang, S. Liu, J. Li, S.-X. Zhang, and S. Yin, Relaxation critical dynamics in measurement-induced phase transitions, *arXiv:2502.13408* (2025).
- [69] K. Khanna, A. Kumar, R. Vasseur, and A. W. W. Ludwig, Random quantum circuits with time-reversal symmetry, *arXiv:2501.13161* (2025).
- [70] G. Xu and Y.-X. Zhang, Multipartite greenberger-horne-zeilinger entanglement in monitored random clifford circuits, *arXiv:2407.03206* (2025).
- [71] Z. Li and Z.-X. Luo, Exact, Average, and Broken Symmetries in a Simple Adaptive Monitored Circuit, *Quantum* **9**, 1771 (2025).
- [72] H. Tang, H.-Y. Wang, Z. Wang, and X.-L. Qi, Measurement induced scrambling and emergent symmetries in random circuits, *arXiv:2506.18121* (2025).
- [73] Q. Tang and W. Zhu, Measurement-induced phase transition: A case study in the nonintegrable model by density-matrix renormalization group calculations, *Phys. Rev. Res.* **2**, 013022 (2020).
- [74] S.-K. Jian, C. Liu, X. Chen, B. Swingle, and P. Zhang, Measurement-induced phase transition in the monitored sachdev-ye-kitaev model, *Phys. Rev. Lett.* **127**, 140601 (2021).
- [75] X. Turkeshi, A. Biella, R. Fazio, M. Dalmonte, and M. Schirò, Measurement-induced entanglement transitions in the quantum ising chain: From infinite to zero clicks, *Phys. Rev. B* **103**, 224210 (2021).
- [76] P. Sierant, G. Chiriaco, F. M. Surace, S. Sharma, X. Turkeshi, M. Dalmonte, R. Fazio, and G. Pagano, Dissipative Floquet Dynamics: from Steady State to Measurement Induced Criticality in Trapped-ion Chains, *Quantum* **6**, 638 (2022).
- [77] Z. Weinstein, R. Sajith, E. Altman, and S. J. Garratt, Nonlocality and entanglement in measured critical quantum ising chains, *Phys. Rev. B* **107**, 245132 (2023).
- [78] Y. Fuji and Y. Ashida, Measurement-induced quantum criticality under continuous monitoring, *Phys. Rev. B* **102**, 054302 (2020).
- [79] O. Lunt and A. Pal, Measurement-induced entanglement transitions in many-body localized systems, *Phys. Rev. Res.* **2**, 043072 (2020).
- [80] Q. Tang, X. Chen, and W. Zhu, Quantum criticality in the nonunitary dynamics of $(2 + 1)$ -dimensional free fermions, *Phys. Rev. B* **103**, 174303 (2021).
- [81] S.-K. Jian and B. Swingle, Phase transition in von Neumann entropy from replica symmetry breaking, *JHEP* **11**, 221 (2023).
- [82] A. Biella and M. Schirò, Many-body quantum zeno effect and measurement-induced subradiance transition, *Quantum* **5**, 528 (2021).
- [83] G. S. Bentsen, S. Sahu, and B. Swingle, Measurement-induced purification in large- n hybrid brownian circuits, *Phys. Rev. B* **104**, 094304 (2021).
- [84] M. Buchhold, Y. Minoguchi, A. Altland, and S. Diehl, Effective theory for the measurement-induced phase transition of dirac fermions, *Phys. Rev. X* **11**, 041004 (2021).
- [85] P. Sierant and X. Turkeshi, Universal behavior beyond multifractality of wave functions at measurement-induced phase transitions, *Phys. Rev. Lett.* **128**, 130605 (2022).
- [86] X. Yu and X.-L. Qi, Measurement-Induced Entanglement Phase Transition in Random Bilocal Circuits, *arXiv:2201.12704* (2022).
- [87] P. Zhang, C. Liu, S.-K. Jian, and X. Chen, Universal Entanglement Transitions of Free Fermions with Long-range Non-unitary Dynamics, *Quantum* **6**, 723 (2022).
- [88] S. Sahu, S.-K. Jian, G. Bentsen, and B. Swingle, Entanglement phases in large- n hybrid brownian circuits with long-range couplings, *Phys. Rev. B* **106**, 224305 (2022).
- [89] T. Müller, S. Diehl, and M. Buchhold, Measurement-induced dark state phase transitions in long-ranged fermion systems, *Phys. Rev. Lett.* **128**, 010605 (2022).
- [90] T. Minato, K. Sugimoto, T. Kuwahara, and K. Saito, Fate of measurement-induced phase transition in long-

- range interactions, *Phys. Rev. Lett.* **128**, 010603 (2022).
- [91] K. Li, Z.-C. Liu, and Y. Xu, Disorder-induced entanglement phase transitions in non-hermitian systems with skin effects, [arXiv:2305.12342](#) (2023).
- [92] X. Feng, S. Liu, S. Chen, and W. Guo, Absence of logarithmic and algebraic scaling entanglement phases due to the skin effect, *Phys. Rev. B* **107**, 094309 (2023).
- [93] X. Sun, H. Yao, and S.-K. Jian, New critical states induced by measurement, [arXiv:2301.11337](#) (2023).
- [94] G. Chiriacò, M. Tsitsishvili, D. Poletti, R. Fazio, and M. Dalmonte, Diagrammatic method for many-body non-markovian dynamics: Memory effects and entanglement transitions, *Phys. Rev. B* **108**, 075151 (2023).
- [95] S. J. Garratt, Z. Weinstein, and E. Altman, Measurements conspire nonlocally to restructure critical quantum states, *Phys. Rev. X* **13**, 021026 (2023).
- [96] E. V. H. Doggen, Y. Gefen, I. V. Gornyi, A. D. Mirlin, and D. G. Polyakov, Evolution of many-body systems under ancilla quantum measurements, *Phys. Rev. B* **107**, 214203 (2023).
- [97] M. Tsitsishvili, D. Poletti, M. Dalmonte, and G. Chiriacò, Measurement induced transitions in non-Markovian free fermion ladders, *SciPost Phys. Core* **7**, 011 (2024).
- [98] Y.-P. Wang, C. Fang, and J. Ren, Absence of measurement-induced entanglement transition due to feedback-induced skin effect, *Phys. Rev. B* **110**, 035113 (2024).
- [99] G. Martín-Vázquez, T. Tolppanen, and M. Silveri, Phase transitions induced by standard and feedback measurements in transmon arrays, *Phys. Rev. B* **109**, 214308 (2024).
- [100] Z.-C. Liu, K. Li, and Y. Xu, Dynamical transition due to feedback-induced skin effect, *Phys. Rev. Lett.* **133**, 090401 (2024).
- [101] X. Feng and S. Chen, Delocalization of skin steady states, *Phys. Rev. B* **110**, 144305 (2024).
- [102] E. V. H. Doggen, I. V. Gornyi, and A. D. Mirlin, Ancilla quantum measurements on interacting chains: Sensitivity of entanglement dynamics to the type and concentration of detectors, *Phys. Rev. B* **109**, 224203 (2024).
- [103] X. Huang, H.-Z. Li, Y.-J. Zhao, S. Liu, and J.-X. Zhong, Quantum feedback induced entanglement relaxation and dynamical phase transition in monitored free fermion chains with a wannier-stark ladder, *Phys. Rev. B* **111**, 184302 (2025).
- [104] H.-Z. Li, J.-X. Zhong, and X.-J. Yu, Measurement-induced entanglement phase transition in free fermion systems, *Journal of Physics: Condensed Matter* **37**, 273002 (2025).
- [105] V. Ravindranath, Z.-C. Yang, and X. Chen, Free fermions under adaptive quantum dynamics, *Quantum* **9**, 1685 (2025).
- [106] Z. Xiao, T. Ohtsuki, and K. Kawabata, Universal stochastic equations of monitored quantum dynamics, *Phys. Rev. Lett.* **134**, 140401 (2025).
- [107] S. Gopalakrishnan, E. McCulloch, and R. Vasseur, Monitored fluctuating hydrodynamics, [arXiv:2504.02734](#) (2025).
- [108] C. Muzzi, M. Tsitsishvili, and G. Chiriacò, Entanglement enhancement induced by noise in inhomogeneously monitored systems, *Phys. Rev. B* **111**, 014312 (2025).
- [109] M. S. Foster, H. Guo, C.-M. Jian, and A. W. W. Ludwig, Free-fermion measurement-induced volume- area-law entanglement transition in the presence of fermion interactions, [arXiv:2510.23706](#) (2025).
- [110] H. Guo, M. S. Foster, C.-M. Jian, and A. W. W. Ludwig, Field theory of monitored interacting fermion dynamics with charge conservation, *Phys. Rev. B* **112**, 064304 (2025).
- [111] Y.-M. Ding, Z. Liu, X. Tian, Z. Wang, Y. Zhu, and Z. Yan, Mixed-state measurement-induced phase transitions in imaginary-time dynamics, [arXiv:2511.04402](#) (2025).
- [112] Z. Xiao and K. Kawabata, Topology of monitored quantum dynamics, [arXiv:2412.06133](#) (2025).
- [113] C. Noel, P. Niroula, D. Zhu, A. Risinger, L. Egan, D. Biswas, M. Cetina, A. V. Gorshkov, M. J. Gullans, D. A. Huse, and C. Monroe, Measurement-induced quantum phases realized in a trapped-ion quantum computer, *Nature Physics* **18**, 760 (2022).
- [114] J. M. Koh, S.-N. Sun, M. Motta, and A. J. Minnich, Measurement-induced entanglement phase transition on a superconducting quantum processor with mid-circuit readout, *Nature Physics* **19**, 1314 (2023).
- [115] J. C. Hoke, M. Ippoliti, E. Rosenberg, D. Abanin, R. Acharya, T. I. Andersen, M. Ansmann, F. Arute, K. Arya, A. Asfaw, J. Atalaya, J. C. Bardin, A. Bengtsson, G. Bortoli, A. Bourassa, J. Bovaird, L. Brill, M. Broughton, B. B. Buckley, D. A. Buell, T. Burger, B. Burkett, N. Bushnell, Z. Chen, B. Chiaro, D. Chik, J. Cogan, R. Collins, P. Conner, W. Courtney, A. L. Crook, B. Curtin, A. G. Dau, D. M. Debroy, A. Del Toro Barba, S. Demura, A. Di Paolo, I. K. Drozdov, A. Dunsworth, D. Eppens, C. Erickson, E. Farhi, R. Fatemi, V. S. Ferreira, L. F. Burgos, E. Forati, A. G. Fowler, B. Foxen, W. Giang, C. Gidney, D. Gilboa, M. Giustina, R. Gosula, J. A. Gross, S. Habegger, M. C. Hamilton, M. Hansen, M. P. Harrigan, S. D. Harrington, P. Heu, M. R. Hoffmann, S. Hong, T. Huang, A. Huff, W. J. Huggins, S. V. Isakov, J. Iveland, E. Jeffrey, Z. Jiang, C. Jones, P. Juhas, D. Kafri, K. Kechedzhi, T. Khattar, M. Khezri, M. Kieferová, S. Kim, A. Kitaev, P. V. Klimov, A. R. Klots, A. N. Korotkov, F. Kostritsa, J. M. Kreikebaum, D. Landhuis, P. Laptev, K.-M. Lau, L. Laws, J. Lee, K. W. Lee, Y. D. Lensky, B. J. Lester, A. T. Lill, W. Liu, A. Locharla, O. Martin, J. R. McClean, M. McEwen, K. C. Miao, A. Mieszala, S. Montazeri, A. Morvan, R. Movassagh, W. Mruczkiewicz, M. Neeley, C. Neill, A. Nersisyan, M. Newman, J. H. Ng, A. Nguyen, M. Nguyen, M. Y. Niu, T. E. O’Brien, S. Omonije, A. Opremcak, A. Petukhov, R. Potter, L. P. Pryadko, C. Quintana, C. Rocque, N. C. Rubin, N. Saei, D. Sank, K. Sankaragomathi, K. J. Satzinger, H. F. Schurkus, C. Schuster, M. J. Shearn, A. Shorter, N. Shutty, V. Shvarts, J. Skrzynny, W. C. Smith, R. Somma, G. Sterling, D. Strain, M. Szalay, A. Torres, G. Vidal, B. Villalonga, C. V. Heidweiller, T. White, B. W. K. Woo, C. Xing, Z. J. Yao, P. Yeh, J. Yoo, G. Young, A. Zalcman, Y. Zhang, N. Zhu, N. Zobrist, H. Neven, R. Babbush, D. Bacon, S. Boixo, J. Hilton, E. Lucero, A. Megrant, J. Kelly, Y. Chen, V. Smelyanskiy, X. Mi, V. Khemani, P. Roushan, and Google Quantum AI and Collaborators, Measurement-induced entanglement and teleportation on a noisy quantum processor, *Nature* **622**, 481 (2023).

- [116] H. Kamakari, J. Sun, Y. Li, J. J. Thio, T. P. Gujarati, M. P. A. Fisher, M. Motta, and A. J. Minnich, Experimental demonstration of scalable cross-entropy benchmarking to detect measurement-induced phase transitions on a superconducting quantum processor, *Phys. Rev. Lett.* **134**, 120401 (2025).
- [117] X. Feng, J. C, S. Kourtis, and B. Skinner, Postselection-free experimental observation of the measurement-induced phase transition in circuits with universal gates, *arXiv:2502.01735* (2025).
- [118] S.-K. Jian, C. Liu, X. Chen, B. Swingle, and P. Zhang, Quantum error as an emergent magnetic field, *arXiv:2106.09635* (2021).
- [119] Z. Weinstein, Y. Bao, and E. Altman, Measurement-induced power-law negativity in an open monitored quantum circuit, *Phys. Rev. Lett.* **129**, 080501 (2022).
- [120] S. Liu, M.-R. Li, S.-X. Zhang, S.-K. Jian, and H. Yao, Universal kardar-parisi-zhang scaling in noisy hybrid quantum circuits, *Phys. Rev. B* **107**, L201113 (2023).
- [121] Y. Li and M. Claassen, Statistical mechanics of monitored dissipative random circuits, *Phys. Rev. B* **108**, 104310 (2023).
- [122] B. C. Dias, D. Perkovic, M. Haque, P. Ribeiro, and P. A. McClarty, Quantum noise as a symmetry-breaking field, *Phys. Rev. B* **108**, L060302 (2023).
- [123] Z. Li, S. Sang, and T. H. Hsieh, Entanglement dynamics of noisy random circuits, *Phys. Rev. B* **107**, 014307 (2023).
- [124] S. Liu, M.-R. Li, S.-X. Zhang, S.-K. Jian, and H. Yao, Noise-induced phase transitions in hybrid quantum circuits, *Phys. Rev. B* **110**, 064323 (2024).
- [125] S. Liu, M.-R. Li, S.-X. Zhang, and S.-K. Jian, Entanglement structure and information protection in noisy hybrid quantum circuits, *Phys. Rev. Lett.* **132**, 240402 (2024).
- [126] D. Qian and J. Wang, Protect measurement-induced phase transition from noise, *Phys. Rev. Lett.* **134**, 020403 (2025).
- [127] Y. Guo and S. Yang, Locally purified density operators for noisy quantum circuits, *Chinese Physics Letters* **41**, 120302 (2024).
- [128] Y. He and T. A. Brun, Measure and forget dynamics in random circuits, *arXiv:2511.21866* (2025).
- [129] I. Lovas, U. Agrawal, and S. Vijay, Quantum coding transitions in the presence of boundary dissipation, *PRX Quantum* **5**, 030327 (2024).
- [130] X. Turkeshi and P. Sierant, Error-resilience phase transitions in encoding-decoding quantum circuits, *Phys. Rev. Lett.* **132**, 140401 (2024).
- [131] D. Qian and J. Wang, Coherent information phase transition in a noisy quantum circuit, *Phys. Rev. B* **112**, L180301 (2025).
- [132] J. Nelson, J. Rajakumar, and M. J. Gullans, Error correction phase transition in noisy random quantum circuits, *arXiv:2510.07512* (2025).
- [133] E. Dallas and P. Zanardi, Nonlocal magic generation and information scrambling in noisy clifford circuits, *arXiv:2509.20566* (2025).
- [134] F. B. Trigueros and J. A. M. Guzman, Nonstabilizerness and error resilience in noisy quantum circuits, *arXiv:2506.18976* (2025).
- [135] M. Bejan, C. McLauchlan, and B. Beri, Dynamical magic transitions in monitored clifford+ t circuits, *PRX Quantum* **5**, 030332 (2024).
- [136] A. Scocco, W.-K. Mok, L. Aolita, M. Collura, and T. Haug, Rise and fall of nonstabilizerness via random measurements, *arXiv:2507.11619* (2025).
- [137] Y. Zhang and Y. Gu, Quantum magic dynamics in random circuits, *arXiv:2410.21128* (2024).
- [138] Z.-Y. Hou, C. Cao, and Z.-C. Yang, Stabilizer entanglement enhances magic injection, *arXiv:2503.20873* (2025).
- [139] A. Paviglianiti, G. Lami, M. Collura, and A. Silva, Estimating nonstabilizerness dynamics without simulating it, *PRX Quantum* **6**, 030320 (2025).
- [140] X. Turkeshi, E. Tirrito, and P. Sierant, Magic spreading in random quantum circuits, *Nature Communications* **16**, 2575 (2025).
- [141] U. Agrawal, A. Zabalo, K. Chen, J. H. Wilson, A. C. Potter, J. H. Pixley, S. Gopalakrishnan, and R. Vasseur, Entanglement and charge-sharpening transitions in $u(1)$ symmetric monitored quantum circuits, *Phys. Rev. X* **12**, 041002 (2022).
- [142] F. Barratt, U. Agrawal, S. Gopalakrishnan, D. A. Huse, R. Vasseur, and A. C. Potter, Field theory of charge sharpening in symmetric monitored quantum circuits, *Phys. Rev. Lett.* **129**, 120604 (2022).
- [143] H. Oshima and Y. Fuji, Charge fluctuation and charge-resolved entanglement in a monitored quantum circuit with $u(1)$ symmetry, *Phys. Rev. B* **107**, 014308 (2023).
- [144] S. Majidy, U. Agrawal, S. Gopalakrishnan, A. C. Potter, R. Vasseur, and N. Y. Halpern, Critical phase and spin sharpening in $su(2)$ -symmetric monitored quantum circuits, *Phys. Rev. B* **108**, 054307 (2023).
- [145] M. N. Ivaki, T. Ojanen, and A. G. Moghaddam, Noise resilience in adaptive and symmetric monitored quantum circuits, *npj Quantum Information* **11**, 111 (2025).
- [146] T. Rakovszky, F. Pollmann, and C. W. von Keyserlingk, Sub-ballistic growth of renyi entropies due to diffusion, *Phys. Rev. Lett.* **122**, 250602 (2019).
- [147] J. Richter, O. Lunt, and A. Pal, Transport and entanglement growth in long-range random clifford circuits, *Phys. Rev. Res.* **5**, L012031 (2023).
- [148] P. Sierant and X. Turkeshi, Controlling entanglement at absorbing state phase transitions in random circuits, *Phys. Rev. Lett.* **130**, 120402 (2023).
- [149] V. Ravindranath, Y. Han, Z.-C. Yang, and X. Chen, Entanglement steering in adaptive circuits with feedback, *Phys. Rev. B* **108**, L041103 (2023).
- [150] T.-C. Lu, Z. Zhang, S. Vijay, and T. H. Hsieh, Mixed-state long-range order and criticality from measurement and feedback, *PRX Quantum* **4**, 030318 (2023).
- [151] N. O’Dea, A. Morningstar, S. Gopalakrishnan, and V. Khemani, Entanglement and absorbing-state transitions in interactive quantum dynamics, *Phys. Rev. B* **109**, L020304 (2024).
- [152] A. Zabalo, J. H. Wilson, M. J. Gullans, R. Vasseur, S. Gopalakrishnan, D. A. Huse, and J. H. Pixley, Infinite-randomness criticality in monitored quantum dynamics with static disorder, *Phys. Rev. B* **107**, L220204 (2023).
- [153] G. Shkolnik, A. Zabalo, R. Vasseur, D. A. Huse, J. H. Pixley, and S. Gazit, Measurement induced criticality in quasiperiodic modulated random hybrid circuits, *Phys. Rev. B* **108**, 184204 (2023).
- [154] H. Ha, A. Pandey, S. Gopalakrishnan, and D. A. Huse, Measurement-induced phase transitions in systems with diffusive dynamics, *Phys. Rev. B* **110**, L140301 (2024).

- [155] A. Nahum, S. Roy, B. Skinner, and J. Ruhman, Measurement and entanglement phase transitions in all-to-all quantum circuits, on quantum trees, and in landau-ginsburg theory, *PRX Quantum* **2**, 010352 (2021).
- [156] M. Block, Y. Bao, S. Choi, E. Altman, and N. Y. Yao, Measurement-induced transition in long-range interacting quantum circuits, *Phys. Rev. Lett.* **128**, 010604 (2022).
- [157] T. Hashizume, G. Bentsen, and A. J. Daley, Measurement-induced phase transitions in sparse non-local scramblers, *Phys. Rev. Res.* **4**, 013174 (2022).
- [158] S. Sharma, X. Turkeshi, R. Fazio, and M. Dalmonte, Measurement-induced criticality in extended and long-range unitary circuits, *SciPost Phys. Core* **5**, 023 (2022).
- [159] M. Ippoliti, M. J. Gullans, S. Gopalakrishnan, D. A. Huse, and V. Khemani, Entanglement phase transitions in measurement-only dynamics, *Phys. Rev. X* **11**, 011030 (2021).
- [160] S. Sang, Y. Li, T. Zhou, X. Chen, T. H. Hsieh, and M. P. Fisher, Entanglement negativity at measurement-induced criticality, *PRX Quantum* **2**, 030313 (2021).
- [161] A. Lavasani, Y. Alavirad, and M. Barkeshli, Measurement-induced topological entanglement transitions in symmetric random quantum circuits, *Nature Physics* **17**, 342 (2021).
- [162] A. Lavasani, Y. Alavirad, and M. Barkeshli, Topological order and criticality in $(2 + 1)$ D monitored random quantum circuits, *Phys. Rev. Lett.* **127**, 235701 (2021).
- [163] S. Sang and T. H. Hsieh, Measurement-protected quantum phases, *Phys. Rev. Res.* **3**, 023200 (2021).
- [164] A. Lavasani, Z.-X. Luo, and S. Vijay, Monitored quantum dynamics and the kitaev spin liquid, *Phys. Rev. B* **108**, 115135 (2023).
- [165] A. Sriram, T. Rakovszky, V. Khemani, and M. Ippoliti, Topology, criticality, and dynamically generated qubits in a stochastic measurement-only kitaev model, *Phys. Rev. B* **108**, 094304 (2023).
- [166] K. Klocke and M. Buchhold, Majorana loop models for measurement-only quantum circuits, *Phys. Rev. X* **13**, 041028 (2023).
- [167] D. Qian and J. Wang, Steering-induced phase transition in measurement-only quantum circuits, *Phys. Rev. B* **109**, 024301 (2024).
- [168] H. Yu and J. Hu, Measurement-driven transitions between area law phases, *Physica Scripta* **100**, 065950 (2025).
- [169] K. Klocke, D. Simm, G.-Y. Zhu, S. Trebst, and M. Buchhold, Entanglement dynamics in monitored kitaev circuits: Loop models, symmetry classification, and quantum lifshitz scaling, *Phys. Rev. B* **111**, 224301 (2025).
- [170] X.-J. Yu, S. Yang, S. Liu, H.-Q. Lin, and S.-K. Jian, Gapless symmetry-protected topological states in measurement-only circuits, [arXiv:2501.03851](https://arxiv.org/abs/2501.03851) (2025).
- [171] M. Szyniszewski, A. Romito, and H. Schomerus, Entanglement transition from variable-strength weak measurements, *Phys. Rev. B* **100**, 064204 (2019).
- [172] F. Eckstein, B. Han, S. Trebst, and G.-Y. Zhu, Robust teleportation of a surface code and cascade of topological quantum phase transitions, *PRX Quantum* **5**, 040313 (2024).
- [173] E. H. Chen, G.-Y. Zhu, R. Verresen, A. Seif, E. Bäumer, D. Layden, N. Tantivasadakarn, G. Zhu, S. Sheldon, A. Vishwanath, S. Trebst, and A. Kandala, Nishimori transition across the error threshold for constant-depth quantum circuits, *Nature Physics* **21**, 161 (2025).
- [174] X. Feng, B. Skinner, and A. Nahum, Measurement-induced phase transitions on dynamical quantum trees, *PRX Quantum* **4**, 030333 (2023).
- [175] V. Ravindranath, Y. Han, and X. Chen, Entanglement transitions in noisy quantum circuits on trees, [arXiv:2503.05027](https://arxiv.org/abs/2503.05027) (2025).
- [176] S. Wang, E. Fontana, M. Cerezo, K. Sharma, A. Sone, L. Cincio, and P. J. Coles, Noise-induced barren plateaus in variational quantum algorithms, *Nature Communications* **12**, 6961 (2021).
- [177] M. Schumann, F. K. Wilhelm, and A. Ciani, Emergence of noise-induced barren plateaus in arbitrary layered noise models, *Quantum Science and Technology* **9**, 045019 (2024).
- [178] A. A. Mele, A. Angrisani, S. Ghosh, S. Khatri, J. Eisert, D. S. FranÅga, and Y. Quek, Noise-induced shallow circuits and absence of barren plateaus, [arXiv:2403.13927](https://arxiv.org/abs/2403.13927) (2024).
- [179] A. Sannia, F. Tacchino, I. Tavernelli, G. L. Giorgi, and R. Zambrini, Engineered dissipation to mitigate barren plateaus, *npj Quantum Information* **10**, 81 (2024).
- [180] B. Ware, A. Deshpande, D. Hangleiter, P. Niroula, B. Fefferman, A. V. Gorshkov, and M. J. Gullans, A sharp phase transition in linear cross-entropy benchmarking, [arXiv:2305.04954](https://arxiv.org/abs/2305.04954) (2023).
- [181] S. Sahu and S.-K. Jian, Phase transitions in sampling and error correction in local brownian circuits, *Phys. Rev. A* **109**, 042414 (2024).
- [182] Z. Cheng and M. Ippoliti, Efficient sampling of noisy shallow circuits via monitored unraveling, *PRX Quantum* **4**, 040326 (2023).
- [183] Z. Chen, Y. Bao, and S. Choi, Optimized trajectory unraveling for classical simulation of noisy quantum dynamics, *Phys. Rev. Lett.* **133**, 230403 (2024).
- [184] S. Cichy, P. K. Faehrmann, L. Bittel, J. Eisert, and H. Pashayan, Classical simulation of noisy quantum circuits via locally entanglement-optimal unravelings, [arXiv:2508.05745](https://arxiv.org/abs/2508.05745) (2025).
- [185] D. Aharonov, X. Gao, Z. Landau, Y. Liu, and U. Vazirani, in *Proceedings of the 55th Annual ACM Symposium on Theory of Computing*, STOC 2023 (Association for Computing Machinery, New York, NY, USA, 2023) p. 945–957.
- [186] Y. Shao, F. Wei, S. Cheng, and Z. Liu, Simulating noisy variational quantum algorithms: A polynomial approach, *Phys. Rev. Lett.* **133**, 120603 (2024).
- [187] A. Angrisani, A. A. Mele, M. S. Rudolph, M. Cerezo, and Z. Holmes, Simulating quantum circuits with arbitrary local noise using pauli propagation, [arXiv:2501.13101](https://arxiv.org/abs/2501.13101) (2025).
- [188] S. un Lee, S. Ghosh, C. Oh, K. Noh, B. Fefferman, and L. Jiang, Classical simulation of noisy random circuits from exponential decay of correlation, [arXiv:2510.06328](https://arxiv.org/abs/2510.06328) (2025).
- [189] Y. Martinez, A. Angrisani, E. Pankovets, O. Fawzi, and D. Stilck França, Efficient simulation of parametrized quantum circuits under nonunitary noise through pauli backpropagation, *Phys. Rev. Lett.* **134**, 250602 (2025).
- [190] G. González-García, J. I. Cirac, and R. Trivedi, Pauli path simulations of noisy quantum circuits beyond average case, *Quantum* **9**, 1730 (2025).

- [191] Z.-L. Li and S.-X. Zhang, The dual role of low-weight pauli propagation: A flawed simulator but a powerful initializer for variational quantum algorithms, [arXiv:2508.06358 \(2025\)](#).
- [192] E. Fontana, M. S. Rudolph, R. Duncan, I. Rungger, and C. CĂrstoiu, Classical simulations of noisy variational quantum circuits, *npj Quantum Information* **11**, 84 (2025).
- [193] S. Sang, Y. Zou, and T. H. Hsieh, Mixed-state quantum phases: Renormalization and quantum error correction, *Phys. Rev. X* **14**, 031044 (2024).
- [194] S. Sang and T. H. Hsieh, Stability of mixed-state quantum phases via finite markov length, *Phys. Rev. Lett.* **134**, 070403 (2025).
- [195] R. Ma, V. Khemani, and S. Sang, Circuit-based characterization of finite-temperature quantum phases and self-correcting quantum memory, [arXiv:2509.15204 \(2025\)](#).
- [196] S. Sang, L. A. Lessa, R. S. K. Mong, T. Grover, C. Wang, and T. H. Hsieh, Mixed-state phases from local reversibility, [arXiv:2507.02292 \(2025\)](#).
- [197] J. Y. Lee, C.-M. Jian, and C. Xu, Quantum criticality under decoherence or weak measurement, *PRX Quantum* **4**, 030317 (2023).
- [198] D. Gu, Z. Wang, and Z. Wang, Spontaneous symmetry breaking in open quantum systems: strong, weak, and strong-to-weak, [arXiv:2406.19381 \(2024\)](#).
- [199] P. Sala, S. Gopalakrishnan, M. Oshikawa, and Y. You, Spontaneous strong symmetry breaking in open systems: Purification perspective, [arXiv:2405.02402 \(2024\)](#).
- [200] Y. Kuno, T. Orito, and I. Ichinose, Intrinsic mixed-state topological order in a stabilizer system under stochastic decoherence: Strong-to-weak spontaneous symmetry breaking from a percolation point of view, *Phys. Rev. B* **111**, 064111 (2025).
- [201] L. A. Lessa, R. Ma, J.-H. Zhang, Z. Bi, M. Cheng, and C. Wang, Strong-to-weak spontaneous symmetry breaking in mixed quantum states, *PRX Quantum* **6**, 010344 (2025).
- [202] Y. Guo, S. Yang, and X.-J. Yu, Quantum strong-to-weak spontaneous symmetry breaking in decohered one-dimensional critical states, *PRX Quantum* **6**, 040311 (2025).
- [203] Z. Wang, Z. Wu, and Z. Wang, Intrinsic mixed-state topological order, *PRX Quantum* **6**, 010314 (2025).
- [204] Y. Guo and S. Yang, Strong-to-weak spontaneous symmetry breaking meets average symmetry-protected topological order, *Phys. Rev. B* **111**, L201108 (2025).
- [205] N. Sun, P. Zhang, and L. Feng, Scheme to detect the strong-to-weak symmetry breaking via randomized measurements, *Phys. Rev. Lett.* **135**, 090403 (2025).
- [206] Z. Liu, L. Chen, Y. Zhang, S. Zhou, and P. Zhang, Diagnosing strong-to-weak symmetry breaking via Wightman correlators, *Communications Physics* **8**, 274 (2025).
- [207] L. Chen, N. Sun, and P. Zhang, Strong-to-weak symmetry breaking and entanglement transitions, *Phys. Rev. B* **111**, L060304 (2025).
- [208] K. Temme, S. Bravyi, and J. M. Gambetta, Error mitigation for short-depth quantum circuits, *Phys. Rev. Lett.* **119**, 180509 (2017).
- [209] Y. Kim, C. J. Wood, T. J. Yoder, S. T. Merkel, J. M. Gambetta, K. Temme, and A. Kandala, Scalable error mitigation for noisy quantum circuits produces competitive expectation values, *Nature Physics* **19**, 752 (2023).
- [210] M. C. Tran, K. Sharma, and K. Temme, Locality and error mitigation of quantum circuits, [arXiv:2303.06496 \(2023\)](#).
- [211] P. Niroula, S. Gopalakrishnan, and M. J. Gullans, Error mitigation thresholds in noisy random quantum circuits, *Phys. Rev. B* **112**, 024206 (2025).
- [212] Y. Bao, R. Fan, A. Vishwanath, and E. Altman, Mixed-state topological order and the errorfield double formulation of decoherence-induced transitions, [arXiv:2301.05687 \(2023\)](#).
- [213] R. Fan, Y. Bao, E. Altman, and A. Vishwanath, Diagnostics of mixed-state topological order and breakdown of quantum memory, *PRX Quantum* **5**, 020343 (2024).
- [214] J. Y. Lee, Exact calculations of coherent information for toric codes under decoherence: Identifying the fundamental error threshold, *Phys. Rev. Lett.* **134**, 250601 (2025).
- [215] R. Niwa and J. Y. Lee, Coherent information for calderbank-shor-steane codes under decoherence, *Phys. Rev. A* **111**, 032402 (2025).
- [216] C. H. Bennett, D. P. DiVincenzo, J. A. Smolin, and W. K. Wootters, Mixed-state entanglement and quantum error correction, *Phys. Rev. A* **54**, 3824 (1996).
- [217] M. Horodecki, P. Horodecki, and R. Horodecki, Mixed-state entanglement and distillation: Is there a “bound” entanglement in nature?, *Phys. Rev. Lett.* **80**, 5239 (1998).
- [218] G. Vidal and R. F. Werner, Computable measure of entanglement, *Phys. Rev. A* **65**, 032314 (2002).
- [219] M. B. Plenio, Logarithmic negativity: A full entanglement monotone that is not convex, *Phys. Rev. Lett.* **95**, 090503 (2005).
- [220] P. Calabrese, J. Cardy, and E. Tonni, Entanglement negativity in quantum field theory, *Phys. Rev. Lett.* **109**, 130502 (2012).
- [221] P. Calabrese, J. Cardy, and E. Tonni, Entanglement negativity in extended systems: a field theoretical approach, *Journal of Statistical Mechanics: Theory and Experiment* **2013**, P02008 (2013).
- [222] T.-C. Lu and T. Grover, Singularity in entanglement negativity across finite-temperature phase transitions, *Phys. Rev. B* **99**, 075157 (2019).
- [223] T.-C. Lu, T. H. Hsieh, and T. Grover, Detecting topological order at finite temperature using entanglement negativity, *Phys. Rev. Lett.* **125**, 116801 (2020).
- [224] T.-C. Lu and T. Grover, Entanglement transitions as a probe of quasiparticles and quantum thermalization, *Phys. Rev. B* **102**, 235110 (2020).
- [225] K.-H. Wu, T.-C. Lu, C.-M. Chung, Y.-J. Kao, and T. Grover, Entanglement renyi negativity across a finite temperature transition: A monte carlo study, *Phys. Rev. Lett.* **125**, 140603 (2020).
- [226] H. Shapourian, S. Liu, J. Kudler-Flam, and A. Vishwanath, Entanglement negativity spectrum of random mixed states: A diagrammatic approach, *PRX Quantum* **2**, 030347 (2021).
- [227] B. Collins, Moments and cumulants of polynomial random variables on unitary groups, the itzykson-zuber integral, and free probability, *International Mathematics Research Notices* **2003**, 953 (2003).
- [228] B. Collins and P. Āźniady, Integration with Respect to the Haar Measure on Unitary, Orthogonal and Symplectic Group, *Communications in Mathematical Physics*

- 264, 773 (2006).**
- [229] H. Nishimori, Statistical physics of spin glasses and information processing: an introduction, 111 (Clarendon Press, 2001).
- [230] M. Kardar, Statistical physics of fields (Cambridge University Press, 2007).
- [231] X. Dong, X.-L. Qi, and M. Walter, Holographic entanglement negativity and replica symmetry breaking, *Journal of High Energy Physics* **2021**, 24 (2021).
- [232] Y. Li, S. Vijay, and M. P. Fisher, Entanglement domain walls in monitored quantum circuits and the directed polymer in a random environment, *PRX Quantum* **4**, 010331 (2023).
- [233] S. Boixo, S. V. Isakov, V. N. Smelyanskiy, R. Babbush, N. Ding, Z. Jiang, M. J. Bremner, J. M. Martinis, and H. Neven, Characterizing quantum supremacy in near-term devices, *Nature Physics* **14**, 595 (2018).
- [234] C. Neill, P. Roushan, K. Kechedzhi, S. Boixo, S. V. Isakov, V. Smelyanskiy, A. Megrant, B. Chiaro, A. Dunsworth, K. Arya, R. Barends, B. Burkett, Y. Chen, Z. Chen, A. Fowler, B. Foxen, M. Giustina, R. Graff, E. Jeffrey, T. Huang, J. Kelly, P. Klimov, E. Lucero, J. Mutus, M. Neeley, C. Quintana, D. Sank, A. Vainsencher, J. Wenner, T. C. White, H. Neven, and J. M. Martinis, A blueprint for demonstrating quantum supremacy with superconducting qubits, *Science* **360**, 195 (2018).
- [235] M. Kardar, G. Parisi, and Y.-C. Zhang, Dynamic scaling of growing interfaces, *Phys. Rev. Lett.* **56**, 889 (1986).
- [236] M. Kardar, Roughening by impurities at finite temperatures, *Phys. Rev. Lett.* **55**, 2923 (1985).
- [237] D. A. Huse, C. L. Henley, and D. S. Fisher, Huse, henley, and fisher respond, *Phys. Rev. Lett.* **55**, 2924 (1985).
- [238] P. Hayden and J. Preskill, Black holes as mirrors: quantum information in random subsystems, *Journal of High Energy Physics* **2007**, 120 (2007).
- [239] W. Hou, S. J. Garratt, N. M. Eassa, E. Rosenberg, P. Roushan, Y.-Z. You, and E. Altman, Machine learning the effects of many quantum measurements, [arXiv:2509.08890](https://arxiv.org/abs/2509.08890) (2025).
- [240] H. Kim, A. Kumar, Y. Zhou, Y. Xu, R. Vasseur, and E.-A. Kim, Learning measurement-induced phase transitions using attention, [arXiv:2508.15895](https://arxiv.org/abs/2508.15895) (2025).
- [241] Y. Qing, Y.-Q. Chen, and S.-X. Zhang, Entanglement growth and information capacity in a quasiperiodic system with a single-particle mobility edge, [arXiv:2506.18076](https://arxiv.org/abs/2506.18076) (2025).
- [242] F. Yang, X.-B. Wang, and T. Chen, Bridging measurement-induced phase transition and quantum error correction in monitored quantum circuits with many-body measurements, *Phys. Rev. B* **111**, 064308 (2025).
- [243] R. Morral-Yepes, F. Pollmann, and I. Lovas, Detecting and stabilizing measurement-induced symmetry-protected topological phases in generalized cluster models, *Phys. Rev. B* **108**, 224304 (2023).
- [244] D. Vu, A. Lavasani, J. Y. Lee, and M. P. A. Fisher, Stable measurement-induced floquet enriched topological order, *Phys. Rev. Lett.* **132**, 070401 (2024).
- [245] M. Saffman, T. G. Walker, and K. Mølmer, Quantum information with rydberg atoms, *Rev. Mod. Phys.* **82**, 2313 (2010).
- [246] D. Bluvstein, H. Levine, G. Semeghini, T. T. Wang, S. Ebadi, M. Kalinowski, A. Keesling, N. Maskara, H. Pichler, M. Greiner, V. Vuletić, and M. D. Lukin, A quantum processor based on coherent transport of entangled atom arrays, *Nature* **604**, 451 (2022).
- [247] P. Scholl, A. L. Shaw, R. B.-S. Tsai, R. Finkelstein, J. Choi, and M. Endres, Erasure conversion in a high-fidelity Rydberg quantum simulator, *Nature* **622**, 273 (2023).
- [248] K. Singh, C. E. Bradley, S. Anand, V. Ramesh, R. White, and H. Bernien, Mid-circuit correction of correlated phase errors using an array of spectator qubits, *Science* **380**, 1265 (2023).
- [249] D. Bluvstein, S. J. Evered, A. A. Geim, S. H. Li, H. Zhou, T. Manovitz, S. Ebadi, M. Cain, M. Kalinowski, D. Hangleiter, J. P. Bonilla Ataides, N. Maskara, I. Cong, X. Gao, P. Sales Rodriguez, T. Karolyshyn, G. Semeghini, M. J. Gullans, M. Greiner, V. Vuletić, and M. D. Lukin, Logical quantum processor based on reconfigurable atom arrays, *Nature* **626**, 58 (2024).
- [250] Q. Xu, J. P. Bonilla Ataides, C. A. Pattison, N. Raveendran, D. Bluvstein, J. Wurtz, B. Vasić, M. D. Lukin, L. Jiang, and H. Zhou, Constant-overhead fault-tolerant quantum computation with reconfigurable atom arrays, *Nature Physics* **20**, 1084 (2024).
- [251] H. Bernien, S. Schwartz, A. Keesling, H. Levine, A. Omran, H. Pichler, S. Choi, A. S. Zibrov, M. Endres, M. Greiner, V. Vuletić, and M. D. Lukin, Probing many-body dynamics on a 51-atom quantum simulator, *Nature* **551**, 579 (2017).
- [252] P. Scholl, M. Schuler, H. J. Williams, A. A. Eberharter, D. Barredo, K.-N. Schymik, V. Lienhard, L.-P. Henry, T. C. Lang, T. Lahaye, A. M. Läuchli, and A. Browaeys, Quantum simulation of 2D antiferromagnets with hundreds of Rydberg atoms, *Nature* **595**, 233 (2021).
- [253] S. Ebadi, T. T. Wang, H. Levine, A. Keesling, G. Semeghini, A. Omran, D. Bluvstein, R. Samajdar, H. Pichler, W. W. Ho, S. Choi, S. Sachdev, M. Greiner, V. Vuletić, and M. D. Lukin, Quantum phases of matter on a 256-atom programmable quantum simulator, *Nature* **595**, 227 (2021).
- [254] D. Bluvstein, A. Omran, H. Levine, A. Keesling, G. Semeghini, S. Ebadi, T. T. Wang, A. A. Michailidis, N. Maskara, W. W. Ho, S. Choi, M. Serbyn, M. Greiner, V. Vuletić, and M. D. Lukin, Controlling quantum many-body dynamics in driven rydberg atom arrays, *Science* **371**, 1355 (2021).
- [255] S. Liu, Z. Wu, S.-X. Zhang, and H. Yao, Supersymmetry dynamics on rydberg atom arrays, *Phys. Rev. B* **112**, L020301 (2025).
- [256] X. Wu, X. Liang, Y. Tian, F. Yang, C. Chen, Y.-C. Liu, M. K. Tey, and L. You, A concise review of rydberg atom based quantum computation and quantum simulation*, *Chinese Physics B* **30**, 020305 (2021).
- [257] G. Semeghini, H. Levine, A. Keesling, S. Ebadi, T. T. Wang, D. Bluvstein, R. Verresen, H. Pichler, M. Kalinowski, R. Samajdar, A. Omran, S. Sachdev, A. Vishwanath, M. Greiner, V. Vuletić, and M. D. Lukin, Probing topological spin liquids on a programmable quantum simulator, *Science* **374**, 1242 (2021).

[258] C. Li, S. Liu, H. Wang, W. Zhang, Z.-X. Li, H. Zhai, and Y. Gu, Uncovering emergent spacetime supersym-

metry with rydberg atom arrays, *Phys. Rev. Lett.* **133**, 223401 (2024).